2020-01-01

Oxidation Of Niobium Silicides Obtained By Self-Propagating High-Temperature SynThesis

Frank Anthony Perez
University of Texas at El Paso

OXIDATION OF NIOBIUM SILICIDES OBTAINED BY SELF-PROPAGATING HIGH-TEMPERATURE SYNTHESIS

FRANK ANTHONY PEREZ

Master's Program in Mechanical Engineering

APPROVED:

Evgeny Shafirovich, Ph.D., Chair

Arturo Bronson, Ph.D.

David Roberson, Ph.D.

Stephen L. Crites, Jr., Ph.D.
Dean of the Graduate School

Dedication

Thank you for your constant support and care.

To my Family and friends.

OXIDATION OF NIOBIUM SILICIDES OBTAINED BY SELF-PROPAGATING HIGH-TEMPERATURE SYNTHESIS

by

FRANK ANTHONY PEREZ, B.S.

THESIS

Presented to the Faculty of the Graduate School of

The University of Texas at El Paso

in Partial Fulfillment

of the Requirements

for the Degree of

MASTER OF SCIENCE

Department of Mechanical Engineering

THE UNIVERSITY OF TEXAS AT EL PASO

August 2020

Acknowledgements

I would like to thank my mentor, Dr. Evgeny Shafirovich, for his guidance and his overall help throughout my graduate studies. I am very thankful for all his lessons and support which allowed me to complete this research.

I would like to thank Dr. Arturo Bronson and Dr. David Roberson, who agreed to be part of my thesis committee. I would like to thank my past and present team members at UTEP: Reina Trevino, Alan Esparza, Sergio Cordova, Robert Ferguson, Edgar Maguregui, Gabriel Llausas and all others who have helped me in performing experiments and research insights.

This material is based upon work supported by the Office of Naval Research under award number N00014-17-1-2636.

Abstract

Niobium silicide-based composites are promising materials for high-temperature structural applications, such as gas turbines. One attractive method for their fabrication is mechanically activated self-propagating high-temperature synthesis (MASHS). However, oxidation resistance of niobium silicides produced by MASHS has not been studied yet. In this present work, the oxidation of Nb/Nb_5Si_3 composites obtained by MASHS was investigated by using non-isothermal thermogravimetric analysis (TGA) and differential scanning analysis (DSC). Both techniques have shown that the oxidation starts at about 500 °C and the materials become fully oxidized at 750 – 800 °C. Model-based analysis of the TGA data has shown that the Avrami-Erofeev nucleation and three-dimensional diffusion models exhibit the best fit with the TG curves and predict similar values of the apparent activation energy, 193 and 212 kJ/mol, respectively.

Table of Contents

List of Tables

List of Figures

Chapter 1: Introduction

Developing new materials for high-temperature structural applications is one of important directions in materials science and engineering. Nickel-based superalloys are predominantly used in modern gas turbines for propulsion and power generation. Since their maximum operating temperature is 1150-1200 °C, they are protected by thermal barrier coatings (TBC) and air-cooling systems. The downside to air cooling is that it consumes energy, hence decreasing the overall efficiency. A trend can be observed as increasing the inlet temperature with each engine advancement [1]. The development of novel high-temperature materials would ultimately provide a 50% increase in output power with higher operating temperatures and no auxiliary cooling [2].

Due to a high melting point, low density, high fracture toughness, and good fatigue performance, niobium silicide-based composites are promising candidates for replacing nickel-base superalloys in gas turbines, but their oxidation resistance and creep efficiency must be enhanced [3-5]. This could be achieved by tuning the concentrations of Nb_{ss} and Nb_5Si_3, adding other metals, and using protective coatings.

Innovative powder metallurgy technology is an effective approach to producing a large-scale synthesis of multi-phase microstructures. A promising approach to the fabrication of the niobium silicides is self-propagating high-temperature synthesis (SHS) [6-7]. Figure 1 shows that the SHS process consists of three steps, where the mixture is initially ignited by a localized energy source, such as a heated tungsten wire. Then the combustion front propagates downward forming the new material. Finally, the product is cooled down to room temperature.

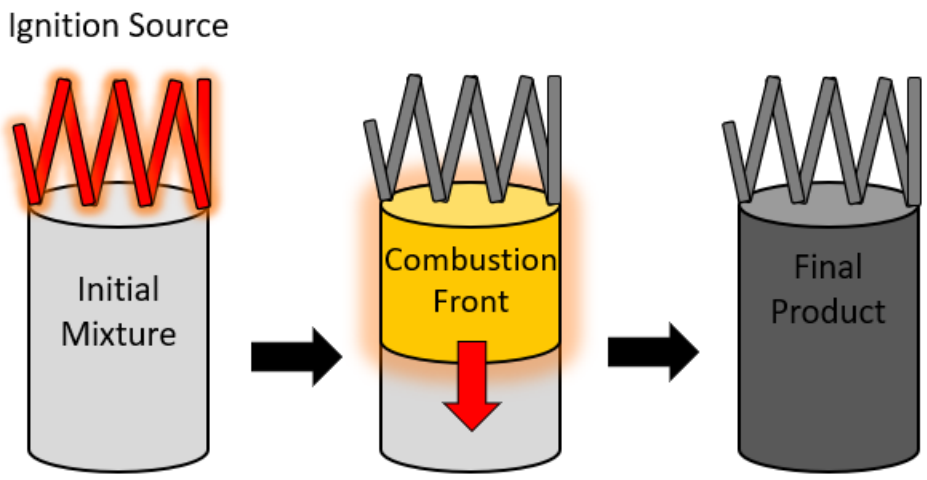

Figure 1: A typical schematic of self-propagating high-temperature synthesis.

However, because of kinetic difficulties, pre-heating is required for SHS of Nb_5Si_3 [8-9]. Another method of allowing SHS of niobium silicides without pre-heating is based on the use of mechanical activation of the reacting mixture. Mechanical activation is a short-term, high-energy ball milling step prior to the SHS process. The milling is usually performed with a planetary ball mill or a shaker ball mill. A powder mixture and balls are placed into a bowl, and the particles are exposed to high-energy ball collisions during the operation of the mill. Mechanical activation has been shown to promote ignition and ensure safe combustion of low-exothermic mixtures. The entire process is commonly referred to as mechanical activation-assisted SHS or mechanically activated SHS (MASHS) [8,9].

The objective of this work was to investigate oxidation of Nb/Nb_5Si_3 composites obtained by MASHS, using non-isothermal thermogravimetric analysis (TGA) and differential scanning calorimetry (DSC). The information on the kinetic models and parameters was extracted from the TGA data with Netzsch Thermokinetics 3.1 software [10].

Chapter 2: Literature Review

2.1 Niobium Silicide-Niobium Composites

The present understanding of phase stability in the niobium silicide-based in situ composites has been developed in parallel with alloy development efforts. Binary Nb-Si alloys with acceptable mechanical properties at low and high temperatures have been studied with insight into their oxidation behavior. Previous investigations have concentrated on Nb-Si alloys, indicating there are three stable niobium silicide phases: Nb_3Si, Nb_5Si_3, and $NbSi_2$ [11-17]. Between them, Nb_5Si_3 has the maximum melting point, 2515 °C, and is thermodynamically stable with niobium, molybdenum and other refractory metals. It makes Nb_5Si_3 a desirable phase for the development of composite materials for high-temperature structural applications.

The Nb-Si binary phase diagram (Figure 2.1) shows two stable phases of Nb_5Si_3: the low-temperature α-phase and the high-temperature β-phase (both are tetragonal) [11]. A metastable-hexagonal γ-phase also exists and can apparently be stabilized by interstitial impurities by Ti and Hf additives [18-21]. Recent computational studies (α, β, γ)-Nb_5Si_3 phases have shown, however, that all these phases are stable, with the α phase exhibiting the highest structural stability [17]. The results on the elastic constants and elastic modulus obtained in that study demonstrate that the α and β phases are fragile, while the γ phase is ductile and has a lower hardness.

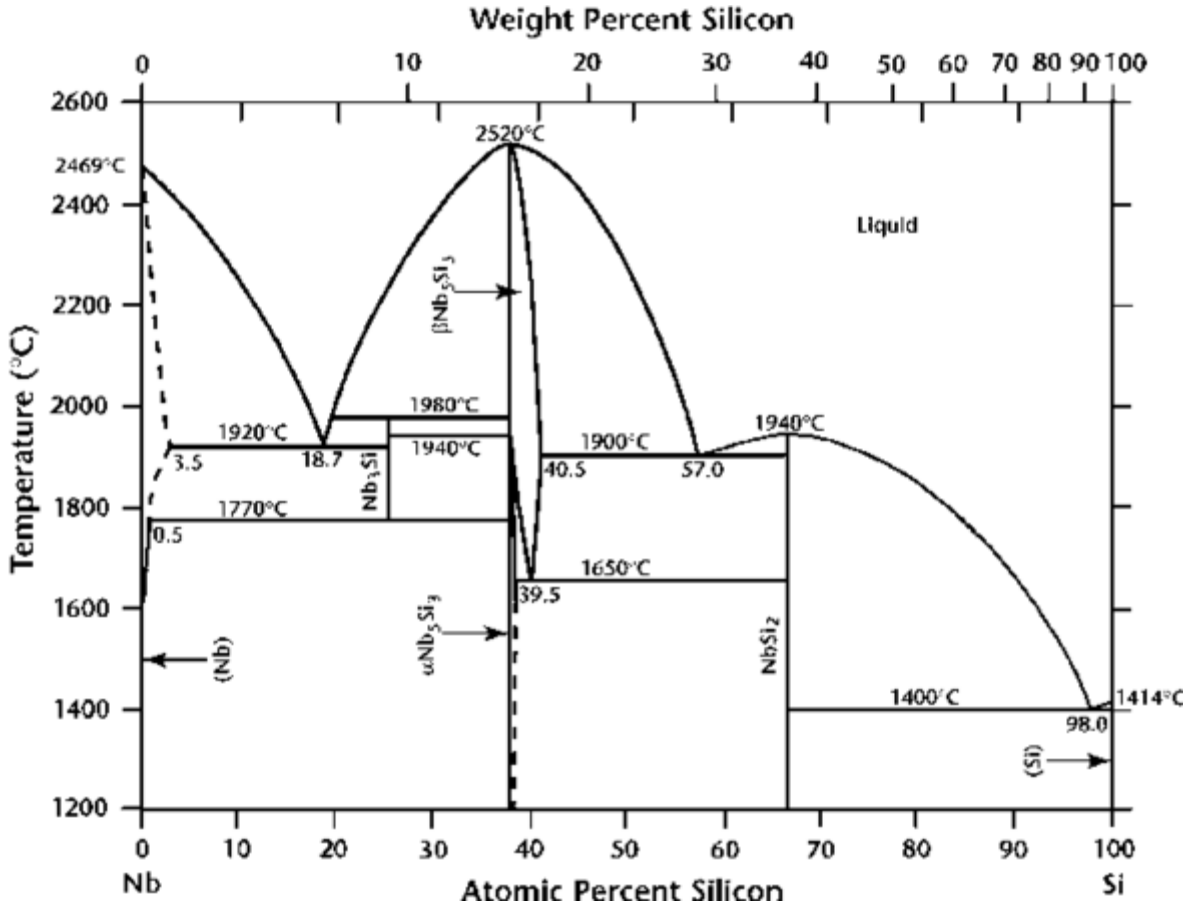

Figure 2.1: Nb-Si binary phase diagram [11].

Niobium silicide-based in-situ composites usually contain 12-20 at% Si [22]. The volume fraction of silicide does change depending on whether the silicide is Nb_5Si_3 or Nb_3Si [22]. Composites tend to solidify with bcc Nb, Nb_3Si, and α-Nb_5Si_3 phases during casting and other high-temperature manufacturing techniques [23-25].

Most binary Nb-Si alloys consist of large primary niobium dendrites and a fine eutectic mixture of Nb_3Si and Nb_5Si_3 phases [24]. The backscattered SEM images of the Nb-Si alloy (Figure 2.2) show a dark contrast associated with the silicide precipitates [25]. The microstructure consists of niobium particles (bright phase), surrounded by a (dark matrix) mixture of α-Nb_5Si_3

and Nb_3Si [25]. The presence of the Nb_3Si phase instead of the Nb_5Si_3 phase in Figure 2.2 (a) indicates that the alloy is in metastable equilibrium in the as-cast condition. For the 1500 °C/3 h, X-ray diffraction analysis revealed a small presence of Nb_5Si_3, a slight growth from the Nb particles was observed within the microstructure (Figure 2.2 (b)). After 100 h heat treatment at 1500 °C, the microstructure exhibited coarsening (Figure 2.2 (c)), with the Nb_3Si phase transforming to Nb_5Si_3. When Nb-Si mixture was given heat treatment prior to arc-melting, Nb_3Si phase was converted to Nb_5Si_3 via a eutectoid transformation.

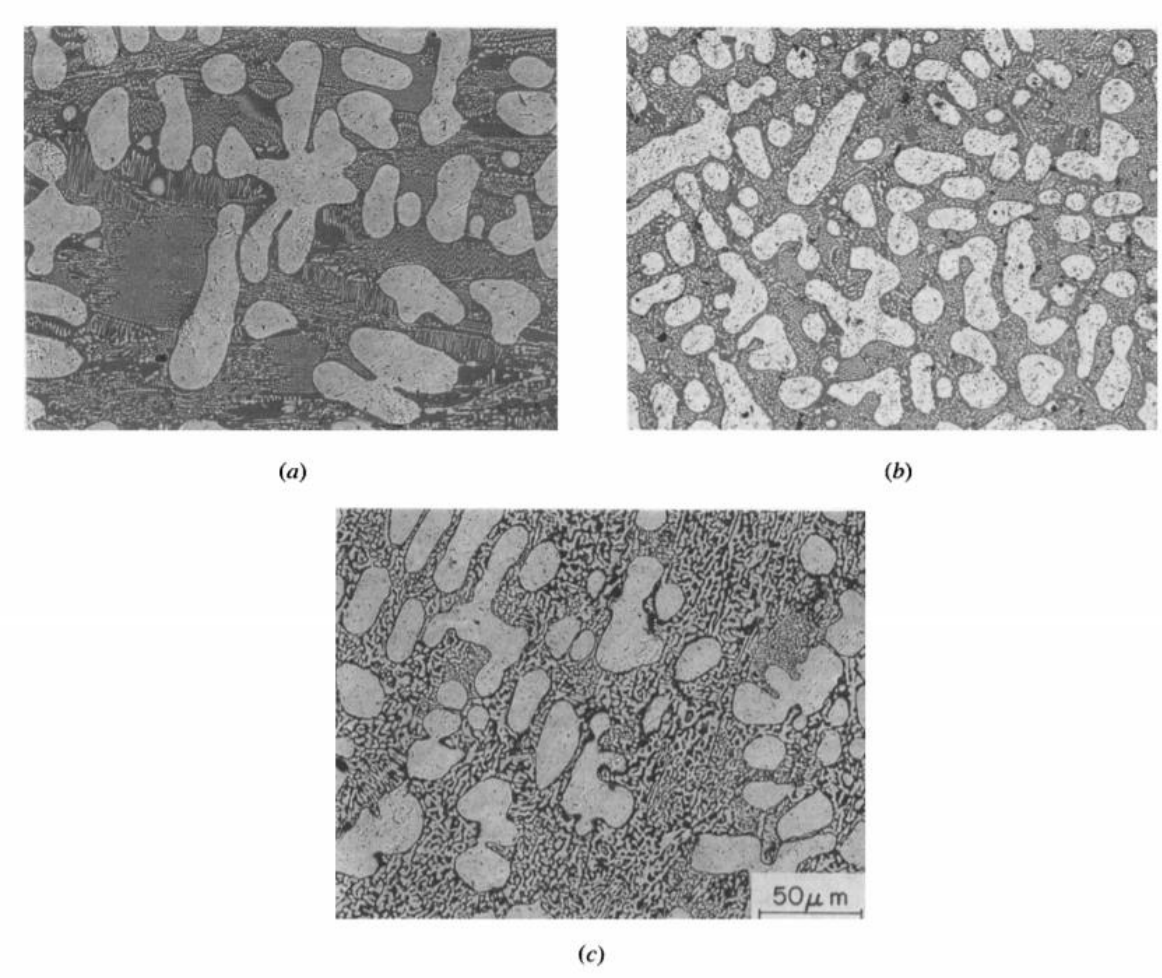

Figure 2.2: Microstructure in the cast Nb-10Si alloy: (a) as-cast; (b) 1500 °C/3 h; and (c) 1500 °C/100 h [25].

Fu et al. [26] have investigated the microstructure of Nb-Si alloys fabricated by spark plasma sintering. It was shown that heat treatment did not influence the phase composition as α-Nb_5Si_3 and β-Nb_5Si_3 phases are observed from the SPS process. As seen in Figure 2.3, two main phases with clear contrast (white and grey phases) exist in all the sintered alloys. The white phase is Nb_{ss}, and the grey phase is Nb_5Si_3.

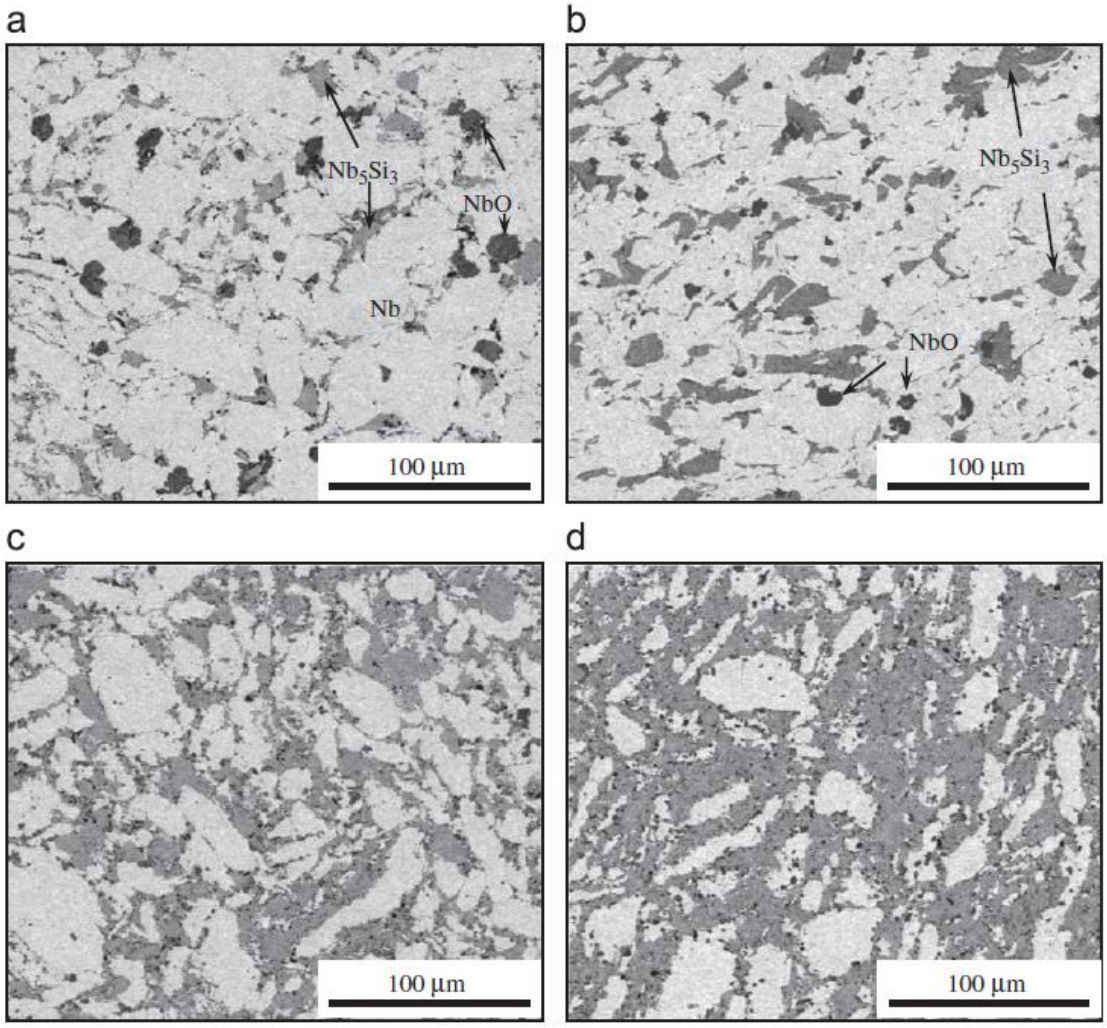

Figure 2.3: Back-scattered electron images of the as-sintered Nb/Nb_5Si_3 samples with volume fraction ratios of 90:10 (a), 80:20 (b), 70:30 (c), 50:50 (d) [26].

2.2 Oxidation of Niobium

High temperature oxidation of metals is demonstrated through series of steps as shown in Figure 2.4 [27]. Oxygen is first adsorbed on the metal surface and then oxide nuclei form in thermodynamically favorable positions on the metal surface. If the activation energy is small enough, the oxygen penetrating into the base material may cause internal oxidation. At the same time, the metal ions continue to diffuse into the developed oxide scales, and this may be coupled with internal diffusing of oxygen [28]. The stresses created by the different thermal expansion coefficients of the oxides can cause a crack in the scale.

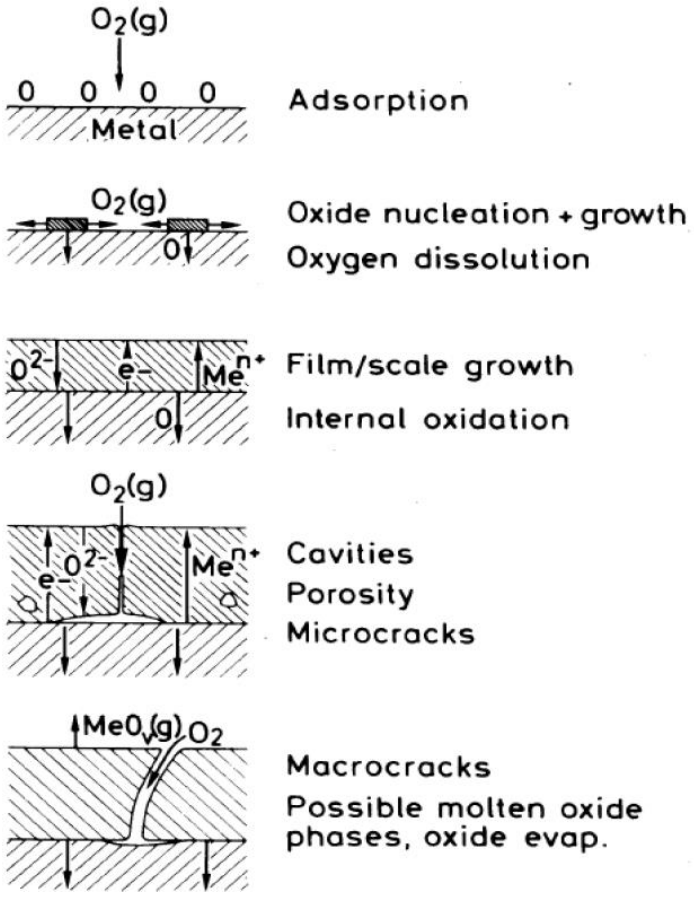

Figure 2.4: Scale formation during high temperature oxidation: (a) O_2 gas absorption, (b) O_2 dissolution, (c) thin oxide film formation, (d) oxide layer growth, and (e) thick oxide layer [27].

The high temperature oxidation of niobium is characterized by inward diffusion of oxygen through the scale. Initially, a protective layer is formed, but, as the scale grows, the formation of oxide at the scale-metal interface stresses the oxide, resulting in the scale cracking and a linear, i.e. non-protective, oxidation [29]. Oxidation of niobium typically correlates with the saturation of the niobium lattice with oxygen. As temperature increases from 500°C to 600°C, NbO and NbO_2 begin to form along the grain boundaries [30]. A third oxide, Nb_2O_5, forms at temperatures above 600 °C and has three different polymorphs [31]. Layers of NbO appear under the α-Nb_2O_5 at temperatures from 600°C to 650 °C, followed by the formation of β-Nb_2O_5 layers at higher temperatures. Monoclinic form of Nb_2O_5 has also been reported [32].

In recently published reports on the oxidation of pure Nb and Nb-based alloys, Nb_2O_5 was observed in the oxide scales [33,34]. Oxidation of Nb is described by the following reaction equations [35]:

$$(4/5)Nb + O_2 = (2/5)Nb_2O_5 \quad (1)$$

$$(24/29)Nb + O_2 = (2/29)Nb_{12}O_{29} \quad (2)$$

$Nb_{12}O_{29}$ appears to be an intermediate reaction product of Nb and oxygen, caused by oxygen deficiency. In addition, as oxidation occurs, the atomic Si present in the Nb_{ss} may produce a protective layer on the alloy through the following reaction:

$$Si + O_2 = SiO_2 \quad (3)$$

The formation of the Nb_2O_5 and the SiO_2 by oxidation of Nb_5Si_3 and Nb_3Si is also possible through the following reactions:

$$(4/37)Nb_5Si_3 + (37/2)\,O_2 = (10/37)Nb_2O_5 + (12/37)\,SiO_2 \quad (4)$$

$$(4)Nb_3Si + (19)O_2 = (6)Nb_2O_5 + (4)SiO_2 \quad (5)$$

The oxidation of metals, alloys, and compounds has been widely studied using thermogravimetry, also called thermogravimetric analysis (TGA) [36, 37]. It is often useful to oxidize samples isothermally and measure the mass gain. In work [38], the effect of tin additive on the oxidation of Nb-24Ti-18Si-5Cr-5Al-2Mo-5Hr alloy (referred as JG4) in air was studied using isothermal TGA. The alloy with tin (JG6) has composition Nb-24Ti-18Si-5Al-5Cr-2Mo-5Hf-5Sn. Both alloys were tested as heat-treated (HT) and as-cast samples (AC). Figure 2.5 shows the thermogravimetric curves obtained at 1200 °C. It is seen that the oxidation of IG6-AC is slower than that of IG4-AC. Similarly, the oxidation of IG6-HT is slower than that of IG4-HT. The analysis of the TG data indicates the linear oxidation law for IG4-AC, while for IH6-AC it was parabolic during the first 9 h and then changed to linear. The positive effect of tin on the oxidation resistance was explained by formation of Nb_3Sn phase at the scale/diffusion zone interface.

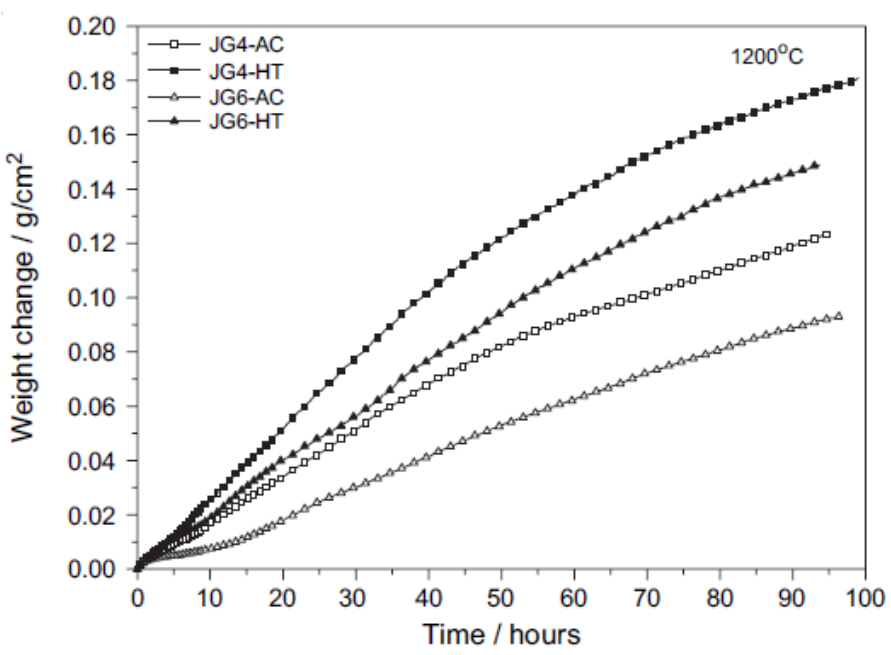

Figure 2.5: TG curves for oxidation of alloys JG4 and JG6 in air at 1200 °C [38].

The kinetics and mechanism of metal oxidation can be investigated using non-isothermal TGA and differential scanning calorimetry (DSC) [39-40]. Kinetic parameters such as the activation energy and pre-exponential factor can be extracted from TGA and DSC data using the Ozawa-Flynn-Wall [41], Kissinger [42], and other *model-free* methods. In the present work, the Ozawa-Wall-Flynn method was used to analyze the obtained TGA data. This method assumes first-order kinetics, leading to the dependence:

$$\frac{d\alpha}{dT} = \frac{1}{\beta} A(1 - \alpha) exp\left(-\frac{E}{RT}\right) \tag{6}$$

where α is the conversion degree, β is the heating rate (the rate at which temperature is raised), A is the pre-exponential factor, E is the activation energy, R is the universal gas constant, and T is the absolute temperature. The Ozawa-Wall-Flynn method function applies linear regression to the data ($\log \beta$, $1/T$) obtained in TGA for a fixed α. The activation energy and pre-exponential factor at constant α are then determined using the equations:

$$E = \left(\frac{R}{b}\right) \frac{\Delta(\log \beta)}{\Delta\left(\frac{1}{T}\right)} \tag{7}$$

$$A = \left(-\frac{\beta R}{E}\right) (\ln(1 - \alpha)) 10^{a} \tag{8}$$

where a and b are the Doyle approximation constants, and β is the heating rate nearest the midpoint of the experimental heating range [43]. The activation energy is determined via assuming the initial value of b is 0.457 K/min and then determined for the obtained value of E/RT_c (T_c is the temperature at constant α for β) with the Doyle approximation constants [43]. Once the iteration process is completed, the pre-exponential factor is determined using Eq. (8), where a is determined from the same table.

A *model-based* analysis of the TG data determines the kinetic model (Table 2.1) that best fits the TG curves. The quality of the calculated fit is determined by performing an F-test, where the algorithm searches for the model with the least variance. The best model is characterized by F_{exp} = 1.0. Table 2.1 shows the general forms of the equations in the kinetic models, used for the description of the solid-phase processes [39].

Table 2.1: Kinetic models for solid-phase processes [40].

Code	Kinetic Model	Kinetic Function $f(\alpha)$
Fn	Reaction of nth order	$0.5/(1-\alpha)^n$
An	Avrami-Erofeev nucleation	$n(1-\alpha)[-\ln(1-\alpha)]^{1/n}$
Bna	Prout-Tompkins autocatalysis	$\alpha^m(1-\alpha)^n$
D1	One-dimensional diffusion	$1/2\alpha$
D2	Two-dimensional diffusion	$[\ln(1-\alpha)]^{-1}$
D3	Three-dimensional diffusion – Jander	$3(1-\alpha)^{2/3}/2(1-(1-\alpha)^{\frac{1}{3}})$
D4	Three-dimensional diffusion – Ginstling-Brounshtein	$(3/2)((1-\alpha)^{-\frac{1}{3}}-1)$

Non-isothermal TGA has been used to characterize oxidation of high-temperature Nb-Si alloys. Nb-Si-B alloys were heated to 1200 °C at heating rates of 5, 10, and 20 °C/min in pure oxygen [44]. As seen in Figure 2.6, oxidation behavior can be divided into three stages. The first stage is the oxidation of Nb_{ss}, described by an *n*-order reaction (Fn). At the second stage (923-993 K), a borosilicate layer forms and impedes the oxidation. Kinetics of the borosilicate formation can formally be described by an *n*-order reaction (Fn), Prout-Tompkins autocatalysis (Bna), or *n*-

dimensional Avrami-Erofeev nucleation (An). Both Prout-Tompkins and Avrami-Erofeev models describe the inhibition as a result of the nucleation and coating of the alloy with the product layer. At the third stage, the silicide phases Nb_3Si, Nb_5SiB and niobium boride Nb_3B_2 were fully oxidized. The limiting event at the third stage is one-dimensional diffusion (D1F), despite the fact that calculated activation energies agree better with the *n*-order reaction (Fn).

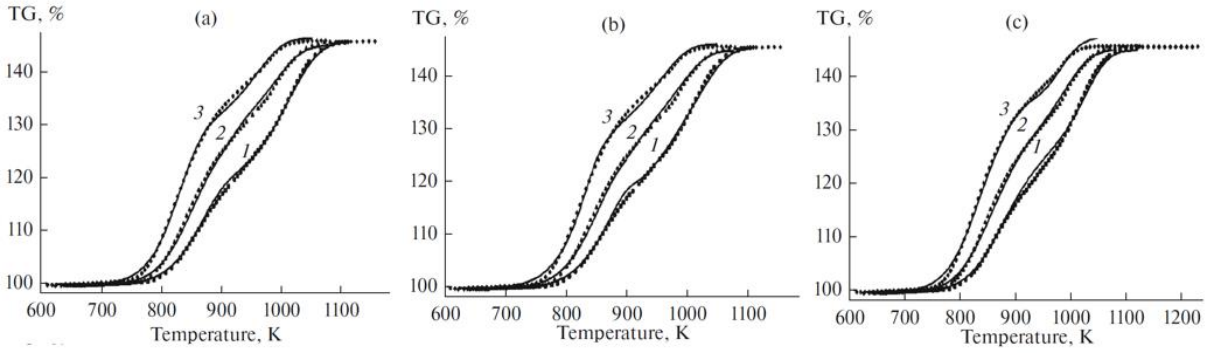

Figure 2.6: Temperature dependences of the weight change under the oxidation of Nb–Si–B alloy in air at heating rates of (1) 19.9, (2) 10.0, and (3) 5.0 K/min; points are the experimental data; lines are calculations by multivariate linear regression according to the models of successive reactions: (a) FnBnaD1F, (b) FnAnD1F, (c) FnFnFn [44].

Chapter 3: Materials and Experimental Methods

3.1 Preparation of Samples

Niobium (−325 mesh, 99.8% pure, Alfa Aesar) and silicon (−325 mesh, 99.5% pure, Alfa Aesar) powders were used as starting materials. To prepare the mixture for synthesis of Nb_5Si_3, the niobium and silicon powders were mixed according to a stoichiometric mole ratio of 5:3. To prepare the mixtures for synthesis of Nb_5Si_3/Nb composites, the mixture ratio was increased accordingly.

3.1.1 Mixing

The powders were mixed in a three-dimensional inversion kinematic tumbler mixer (Inversina 2L, Bioengineering, Figure 3.1). To avoid oxidation, mixing was conducted in a sealed container filled with ultra-high purity argon. The total mass of the prepared mixture was 18.5g in all experiments.

Figure 3.1: Mixer (Inversina 2L, Bioengineering).

3.1.2 Mechanical Activation

The mixed powders were mechanically activated in a high-energy planetary ball mill (Fritsch Pulverisette 7 Premium Line, Figure 3.2.a) using zirconia-coated grinding bowls (Figure 3.2.b) and zirconia grinding balls (diameter: 5 mm). The balls-mixture mass ratio was 5:1. Before milling, the bowls were purged with ultra-high purity argon to avoid oxidation of Nb inside the bowl during mechanical activation. The milling speed was 1000 rpm, and the milling time was 10 min. To prevent high temperatures and reactions during the milling process, a 60-min cooling pause was given after every minute of milling.

Figure 3.2: Milling equipment (a) planetary mill (Fritch Pulverisette 7 Premium Line) and (b) grinding bowl with purging valves.

3.1.3 Compacting

After the milling step, the bowl was opened, and powders were extracted inside a glovebox (Terra Universal, Series 300) in an atmosphere composed of 5% O_2 and 95% N_2. The pressing was conducted in a uniaxial hydraulic press, shown in Fig. 3.3. Powder was deposited within the die (diameter 25 mm) and pressed at 3 metric tons (pressure: 222 MPa). A booster pellet of titanium/boron mixture (1:2 molar ratio, 0.5 g) was compacted at the same pressing parameters to be placed at the top of the sample for an easier and controlled ignition.

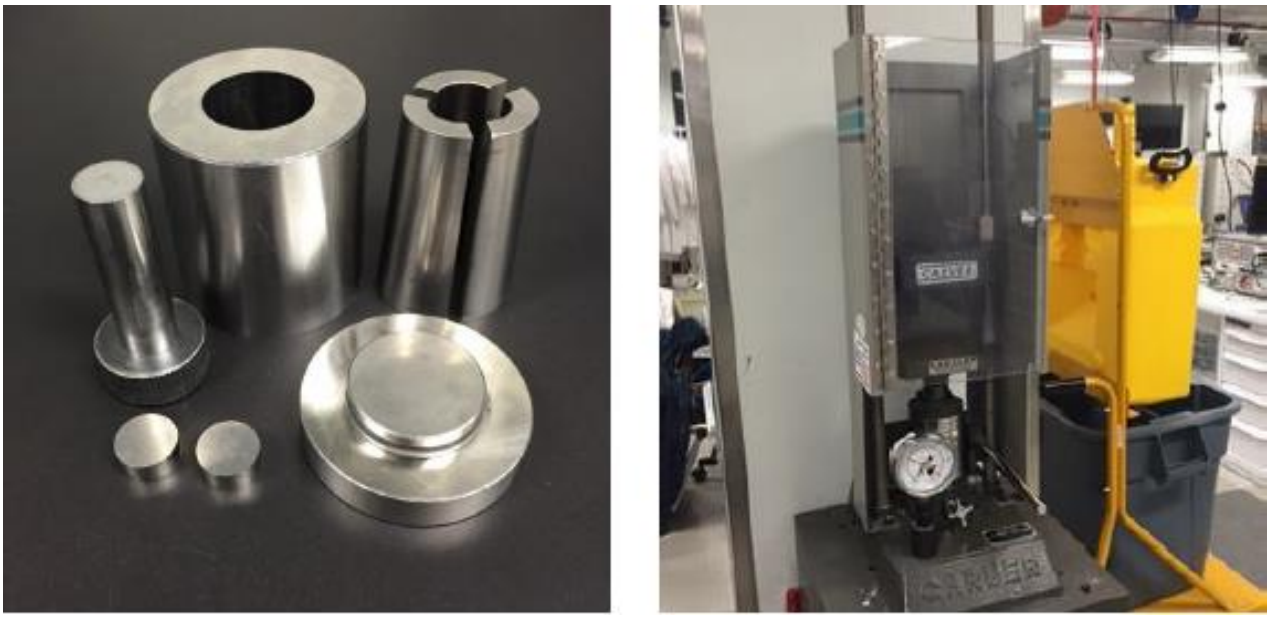

Figure 3.3: Pressing equipment: (a) die set for 13 mm and (b) uniaxial hydraulic press.

3.1.4 Combustion Synthesis

Combustion synthesis was conducted inside a windowed steel chamber (Figure 3.4) connected to a compressed argon cylinder and a vacuum pump. All experiments were conducted in a 1 atm argon environment. The pellet was placed inside the chamber on top of thick thermal paper (Fiberfrax) and ignited using a hand-wound tungsten coil (Midwest Tungsten Service Inc.) heated by a DC power supply (Mastech) set at 15 V.

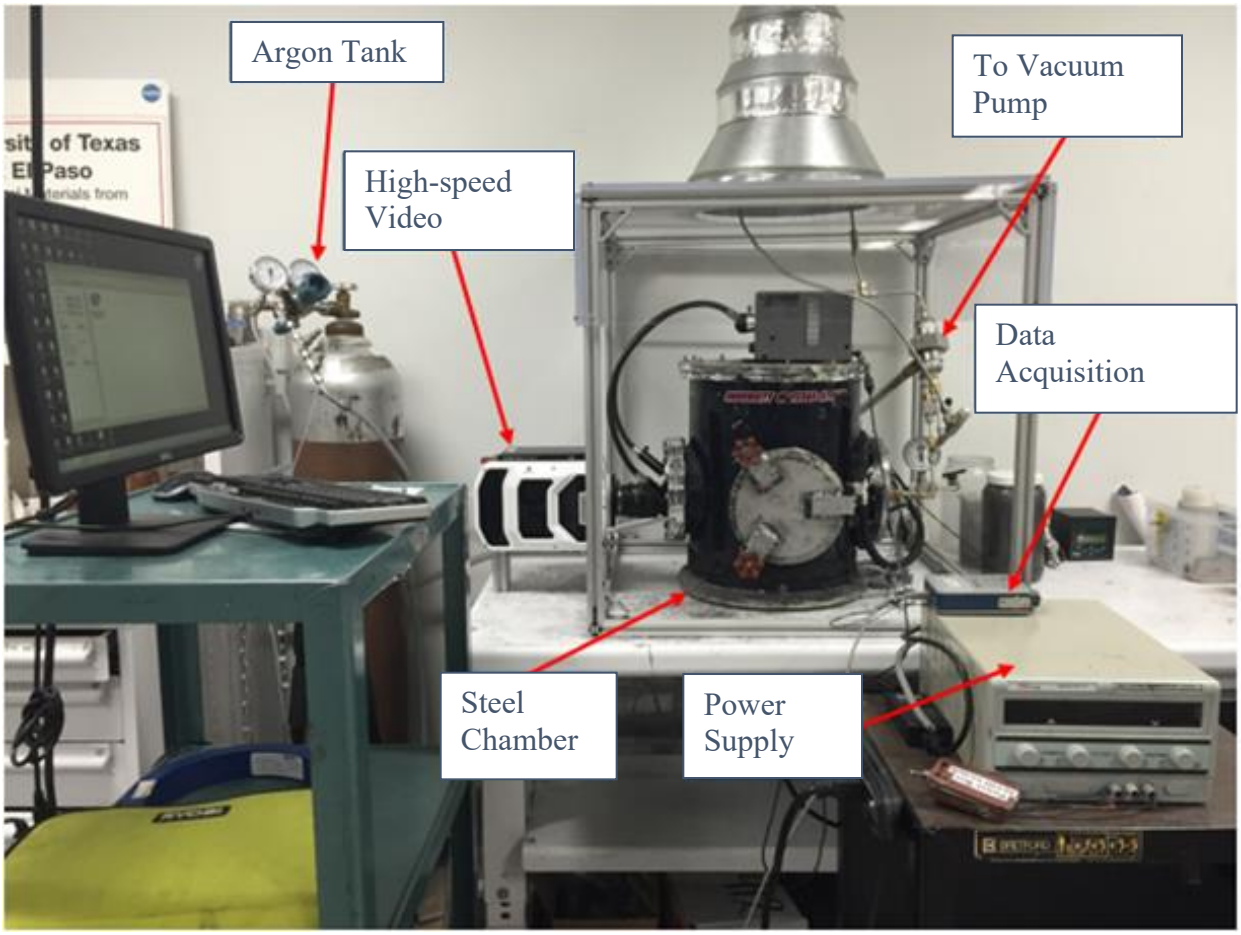

Figure 3.4: Hot-wire ignition setup.

3.2 Characterization Methods

3.2.1 X-ray Diffraction Analysis

The X-ray diffraction analysis was used to examine the powders in search of unwanted reactions during milling and to characterize the phases in the combustion products. Figure 3.5 shows the used instrument (Bruker D8 Discover XRD with Cu K-alpha radiation). The products were crushed into powder and analyzed at 2θ values ranging from 20° to 90°.

Figure 3.5: X-ray diffractometer (Bruker D8 Discover XRD).

3.2.2 Scanning Electron Microscopy (SEM)

To analyze the morphology of the products, samples were examined using a TM-1000 Tabletop Microscope (Figure 3.6.a) and a Hitachi S-4800 Scanning Electron Microscope (Figure 3.6.b). Samples were applied using the "Sprinkle Method" which involves applying water-soluble carbon paste (Electron Microscopy Sciences, CCC Carbon Adhesive) onto the sample holder. Any excess powder was blown off to diminish any contamination within the internal chambers. Polished samples were placed upon electrically conducted non-porous tape (Electron Microscopy Sciences, Conductive Double-sided Carbon Tape).

(a) (b)

Figure 3.6: (a) TM-1000 Tabletop Microscope and (b) Hitachi S-4800 Scanning Electron Microscope.

3.2.3 Thermogravimetric Analysis (TGA)

The Netzsch TGA 209 F1 Iris thermogravimetric analyzer (Figure 3.7) was used to study the oxidation of the obtained products at temperatures up to 1000 °C (the maximum temperature in the instrument). The thermogravimetric analyzer measures the mass of the sample during the linear increase in the temperature. Alumina crucibles (inner diameter 5.85 mm) were used to hold the samples with masses from 10 mg to 69 mg. The oxidation experiments were performed in an oxygen-argon (20% O_2 and 80% Ar) environment. The flow rates of oxygen and argon were 6 mL/min and 24 mL/min, respectively. The tests were conducted at heating rates of 10, 5, 2.5, and 1 °C/min. Netzsch Thermokinetics 3.1 software was used for extraction of kinetic parameters from the TGA data.

Figure 3.7: Thermogravimetric analyzer (Netzsch TGA 209 F1 Iris).

3.2.4 Differential Scanning Calorimetry (DSC)

The Netzsch DSC 404 F1 Pegasus differential scanning calorimeter (Figure 3.8) was used to study the oxidation of the products at temperatures up to 1500 °C. DSC gives information on the released or consumed heat. In this study, exothermic reactions, such as oxidation, are depicted as positive peaks, while endothermic reactions are shown as negative peaks. As in the TGA tests, 5.85 mm alumina crucibles were used to hold the samples with masses from 2 to 5 mg. The oxidation experiments were performed in an oxygen-argon (20% O_2 and 80% Ar) environment. The flow rates of oxygen and argon were 6 mL/min and 24 mL/min, respectively. The heating rate was 10 °C/min.

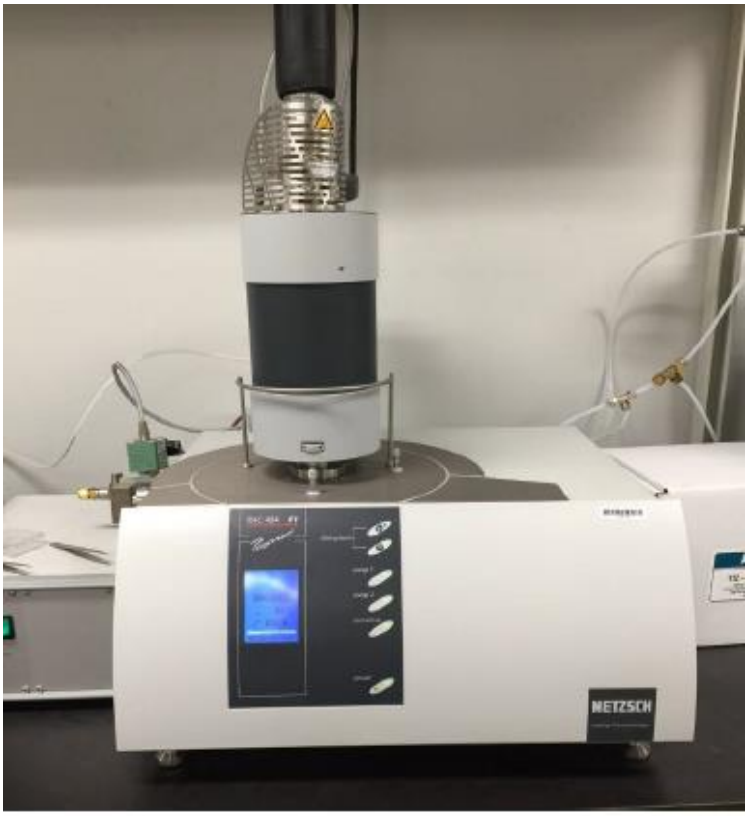

Figure 3.8: Differential scanning calorimeter (Netzsch DSC 404 F1 Pegasus).

Chapter 4: Results and Discussion

4.1 Fabrication of Nb/Nb_5Si_3 Composites

4.1.1 Morphology Analysis of Activated Nb/Si Mixtures

Figure 4.5 shows SEM images of milled Nb/Si mixtures. It can be concluded that not only does milling grind coarse particles that are present in the initial powders, but it also creates a powder that consists of agglomerates where Nb and Si are uniformly mixed. This clearly creates conditions for effective reactions between the two components.

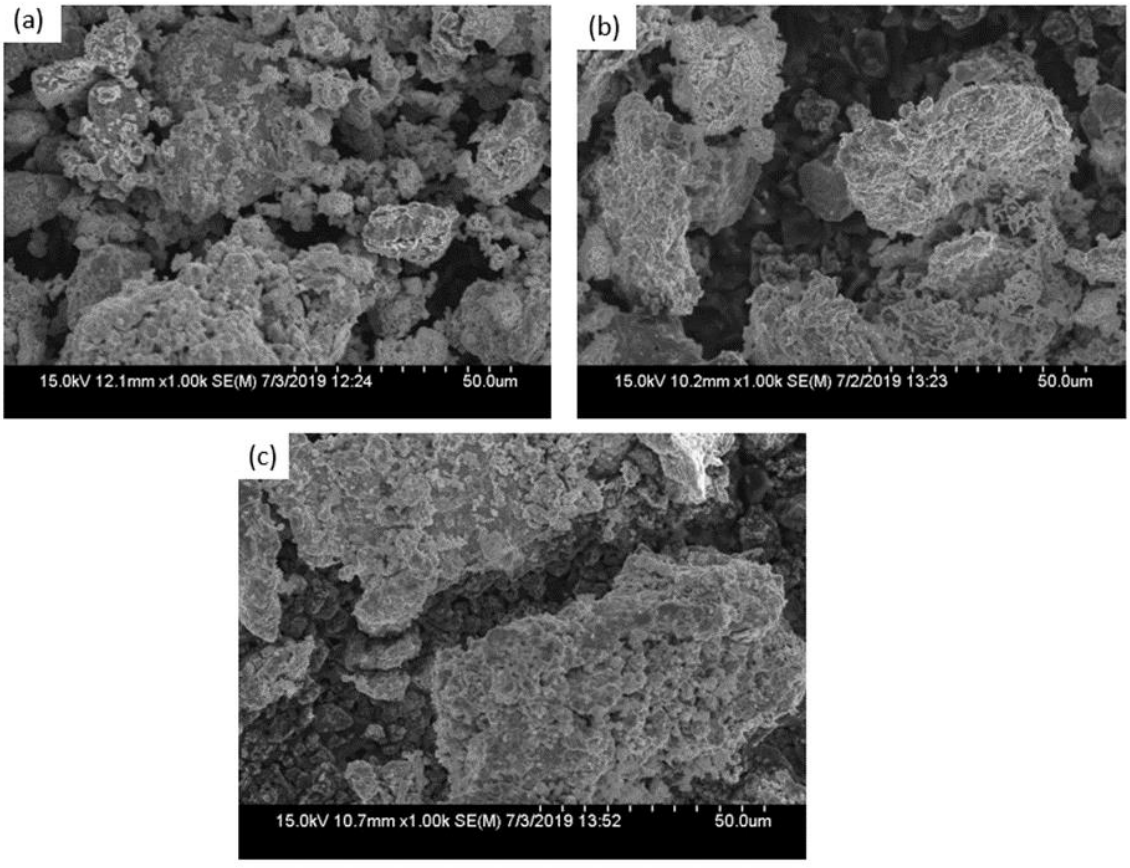

Figure 4.1: SEM images of milled mixtures for the Nb/Si mole ratios of (a) 1.67, (b) 2, and (c) 3.

4.1.2 SHS of Nb/Nb_5Si_3 Products

SHS experiments were conducted with Nb/Si mixtures that had Nb/Si mole ratios of 1.67, 2, and 3. Figure 4.2 shows the images of combustion propagation over pellets compacted from these mixtures. At Nb/Si mole ratios of 1.67 and 2, a steady propagation of a planar combustion front was observed. At Nb/Si ratio of 3, spin combustion took place, where two hot spots were traveling in opposite directions over the pellet surface.

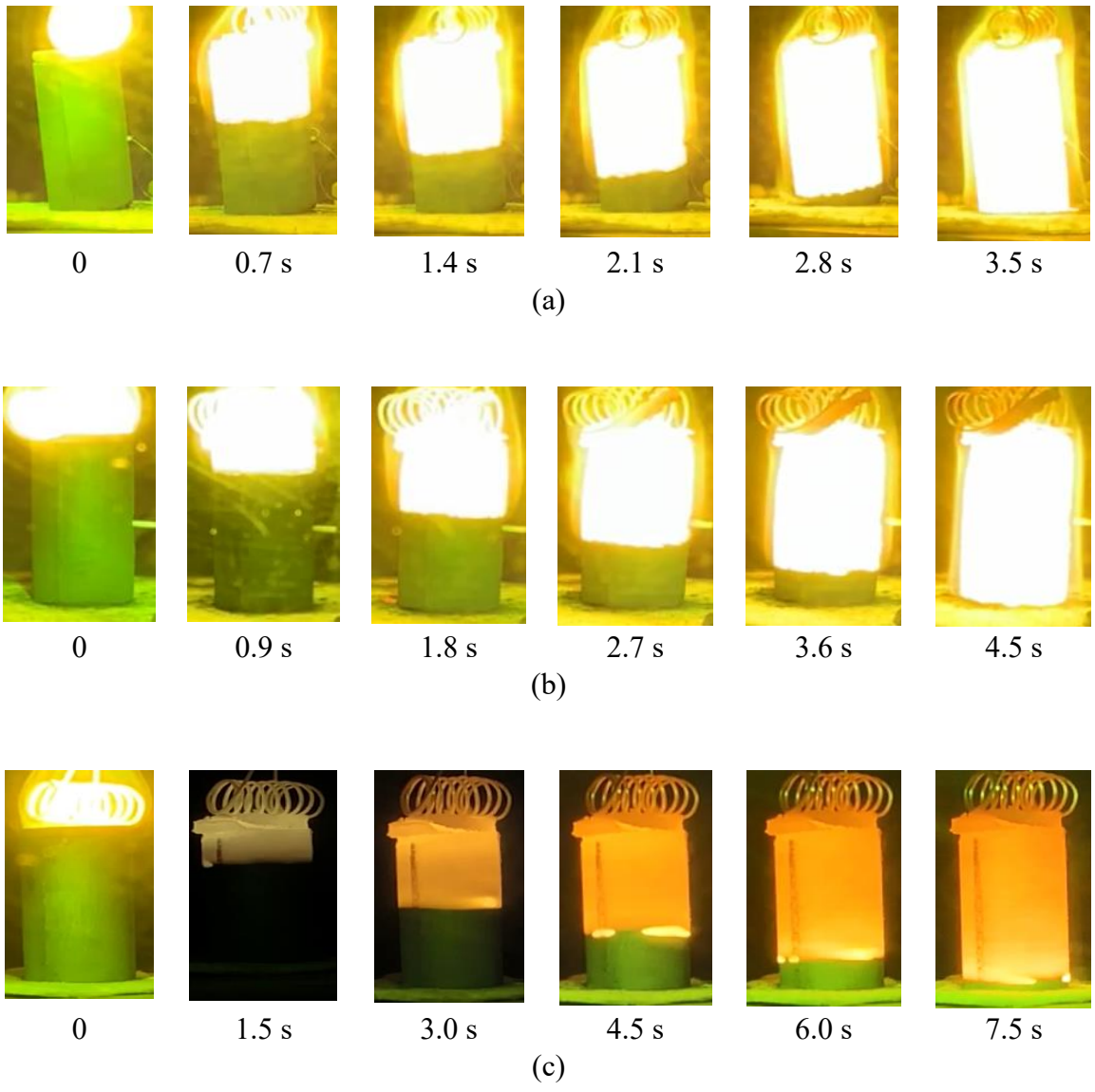

Figure 4.2: Images of combustion propagation over Nb/Si mixture pellets (height: 25±2 mm) with Nb/Si mole ratios of (a) 1.67, (b) 2, and (c) 3. Time zero was selected arbitrarily.

4.1.3 X-ray Diffraction Analysis of Nb/Nb_5Si_3 Products

For XRD analysis, the obtained product pellets were cut into three parts of equal length. The top and bottom of the pellet may be subjected to the so-called end effects. For this reason, only the XRD patterns of the middle parts are shown.

Figure 4.3 shows the XRD pattern of the products obtained by combustion of the mixture with Nb/Si mole ratio of 1.67. The products include α, β, and γ phases of Nb_5Si_3, with traces of Nb_3Si. The α-Nb_5Si_3 is clearly the dominant phase.

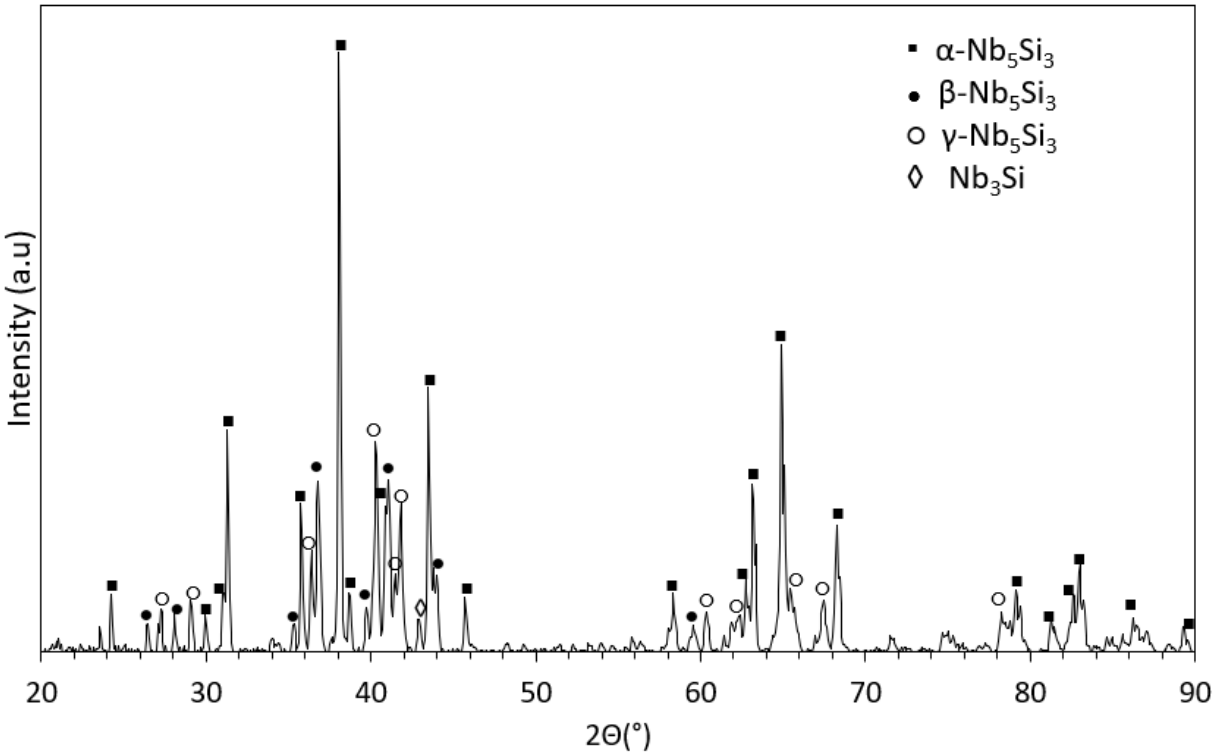

Figure 4.3: XRD pattern of combustion products of the mixture with Nb/Si mole ratio of 1.67 (height of the pellet: 25 mm).

Figure 4.4 shows the XRD pattern of the products obtained by combustion of the mixture with Nb/Si mole ratio of 2. It is seen that the high-temperature β phase disappeared (obviously because the temperature was lower). Niobium is characterized by peaks at 39°, 55°, and 69°. However, the Nb peak at 39° overlaps with α-Nb_5Si_3 peak. The analysis of Nb peaks at 55° and 69° shows that Nb phase is absent at Nb/Si mole ratio of 1.67 (Fig. 4.3) and appears at a ratio of 2. Summarizing, the products of the mixture with Nb/Si mole ratio of 2 include α and γ phases of Nb_5Si_3 as well as Nb, with traces of Nb_3Si.

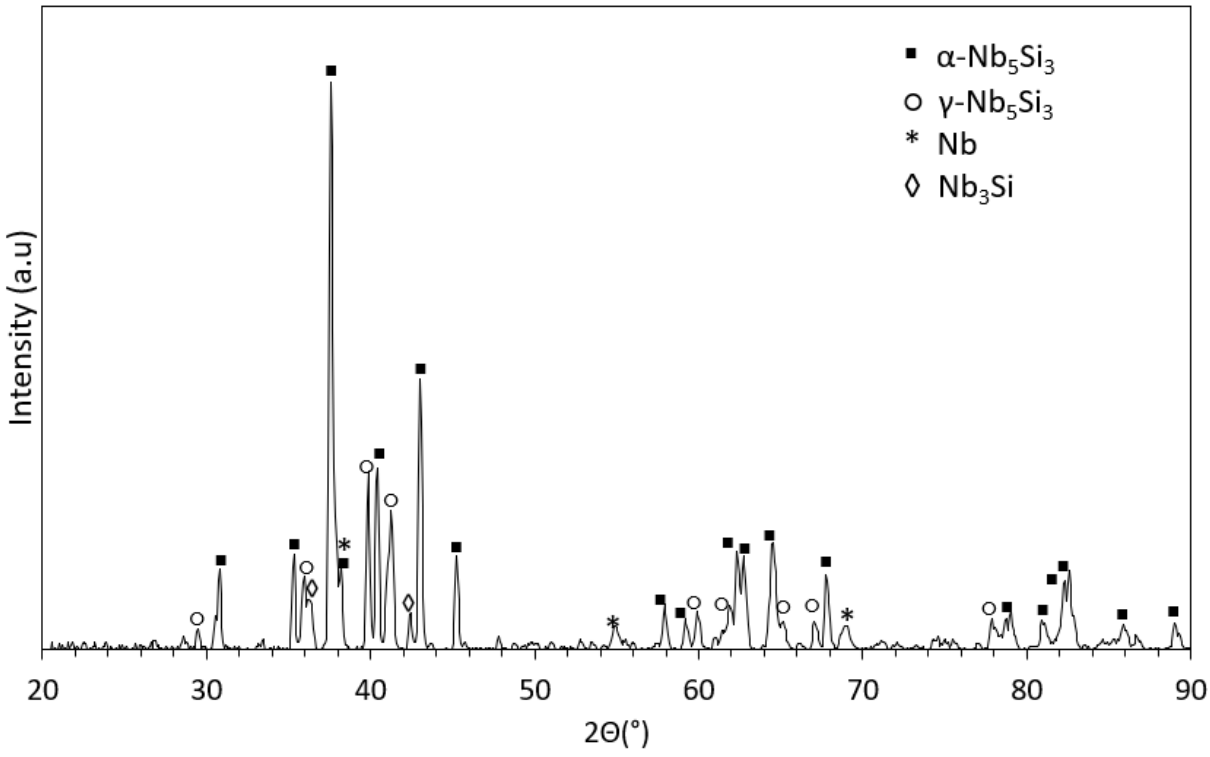

Figure 4.4: XRD pattern of combustion products of the mixture with Nb/Si mole ratio of 2 (height of the pellet: 25 mm).

Figure 4.5 shows the XRD pattern of the products obtained by combustion of the mixture with Nb/Si mole ratio of 3. The α-Nb_5Si_3 was the dominant phase, and the peaks of γ phase became much smaller. The comparison of Nb peaks at 55° and 69° in Figs. 4.4 and 4.5 shows that the content of Nb phase increases with increasing Nb/Si mole ratio from 2 to 3.

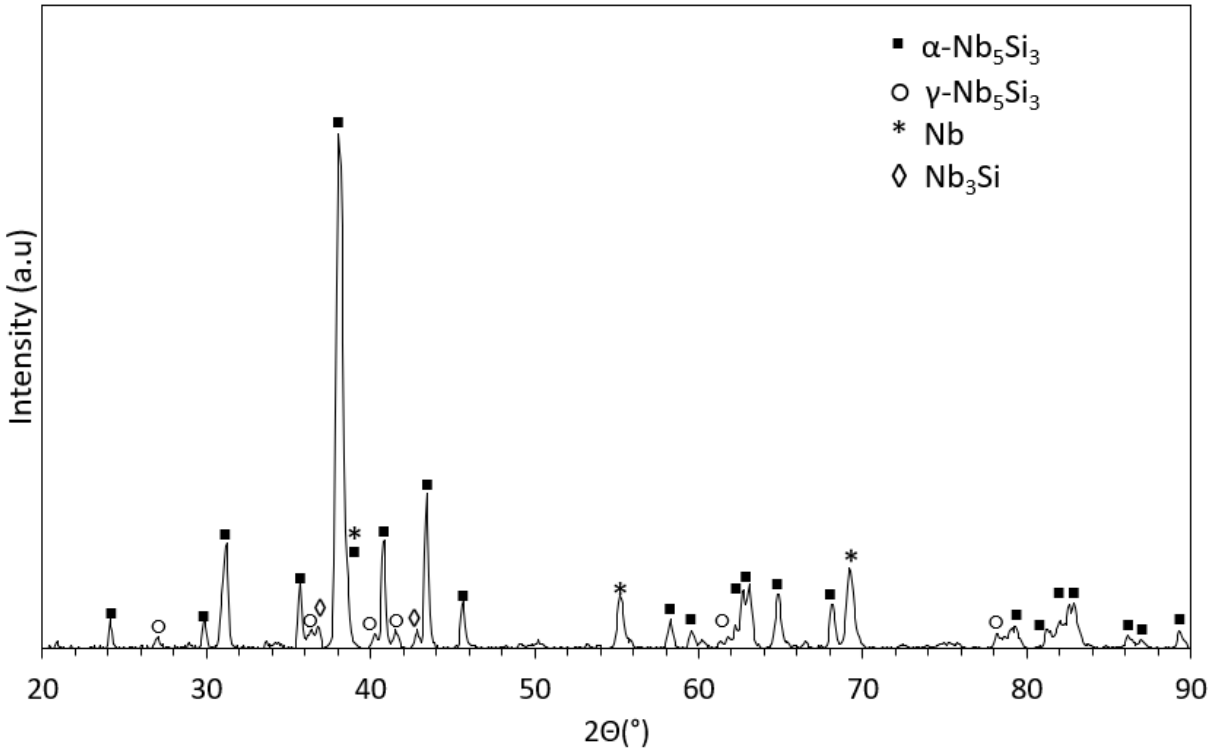

Figure 4.5: XRD pattern of combustion products of the mixture with Nb/Si mole ratio of 3 (height of the pellet: 25 mm).

4.1.4 Morphology Analysis of Nb/Nb_5Si_3 Products

Figure 4.6 shows the microstructures of the products obtained by combustion of the mixtures with Nb/Si mole ratios of 1.67, 2, and 3. Apparently, the dark-grey phases are Nb_5Si_3, and light-grey phases are Nb solid solution (Nb_{ss}). A small amount of Nb is seen even in the products obtained from the stoichiometric 5Nb/3Si mixture (it was not detected by XRD, see Fig. 4.3). All the images also reveal pores.

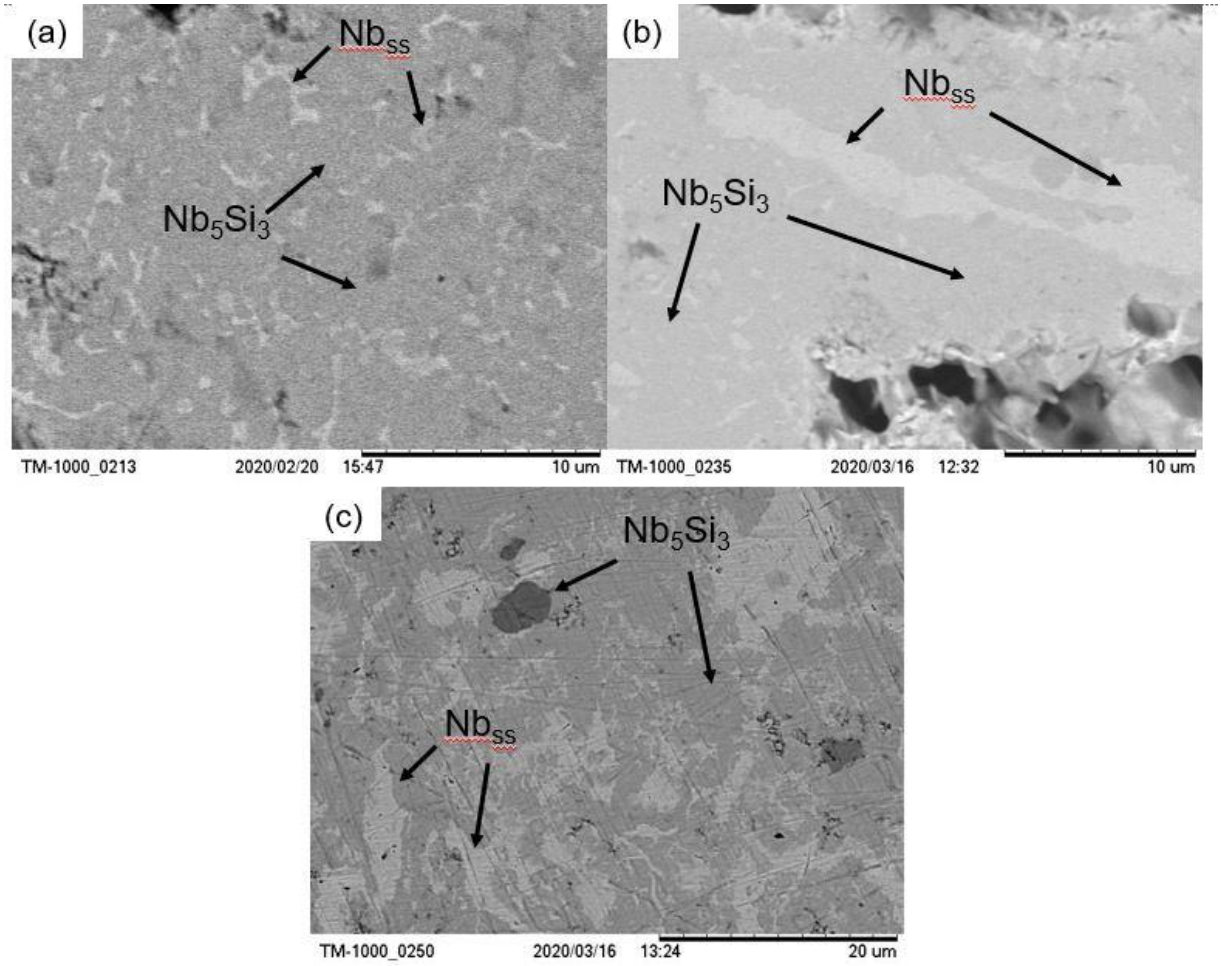

Figure 4.6: SEM images of microstructures for the Nb/Si mole ratios of (a) 1.67, (b) 2, and (c) 3.

4.2 Oxidation of Nb/Nb_5Si_3 Composites

4.2.1 X-ray Diffraction Analysis

Figures 4.7 – 4.9 show the XRD patterns of the obtained Nb/Nb_5Si_3 products after oxidation in TGA experiments. It is seen that the patterns are similar to each other. Nb_2O_5 includes both orthorhombic and monoclinic phases. A small peak at 39° may indicate the presence of non-oxidized Nb, but it could also belong to Nb_2O_5. The molar volume of the monoclinic Nb_2O_5 is 58.3 cm^3, while that of Nb is 10.9 cm^3, suggesting the volume expansion on oxidation of Nb is large [35]. Elemental Si has the most intensive lines at around 28°, followed by the lines at 47° and 56°. Since these lines overlap with strong lines of Nb_2O_5, it is difficult to determine whether there is a non-oxidized Si in the sample. Small traces of SiO_2 can be classified as Cristobalite from the XRD analysis. In any case, it is clear that the products were heavily oxidized.

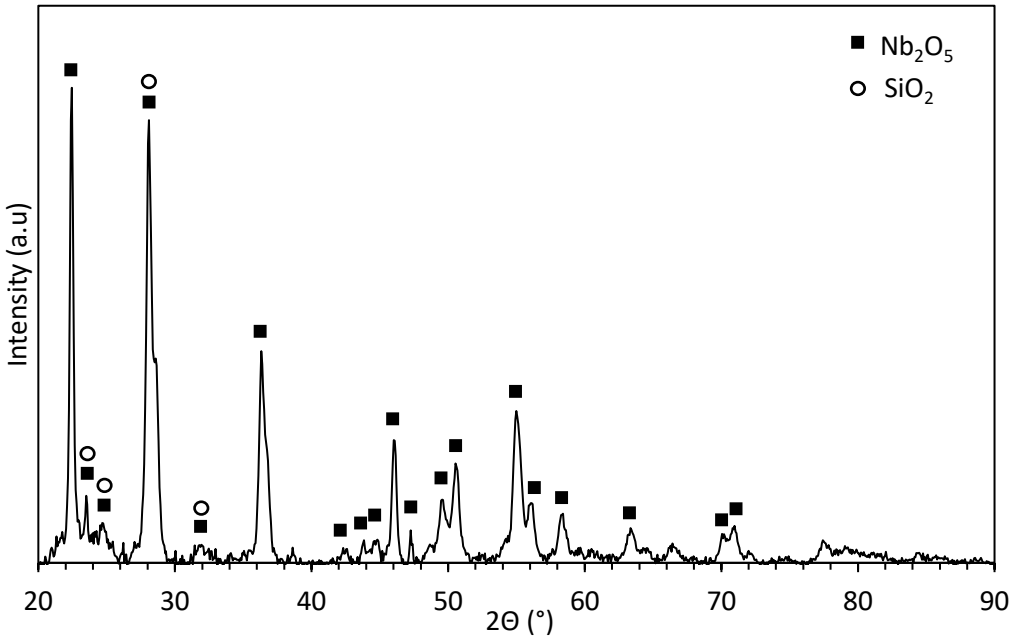

Figure 4.7: XRD pattern of combustion product of the mixture with Nb/Si mole ratio of 1.67 after oxidation in TGA.

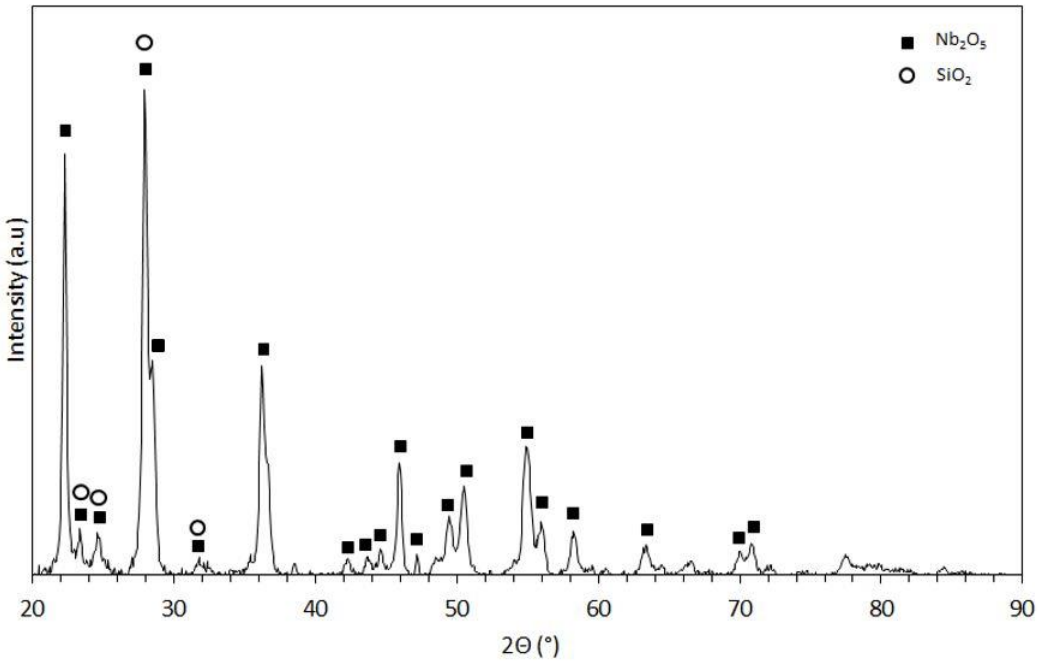

Figure 4.8: XRD pattern of combustion product of the mixture with Nb/Si mole ratio of 2 after oxidation in TGA.

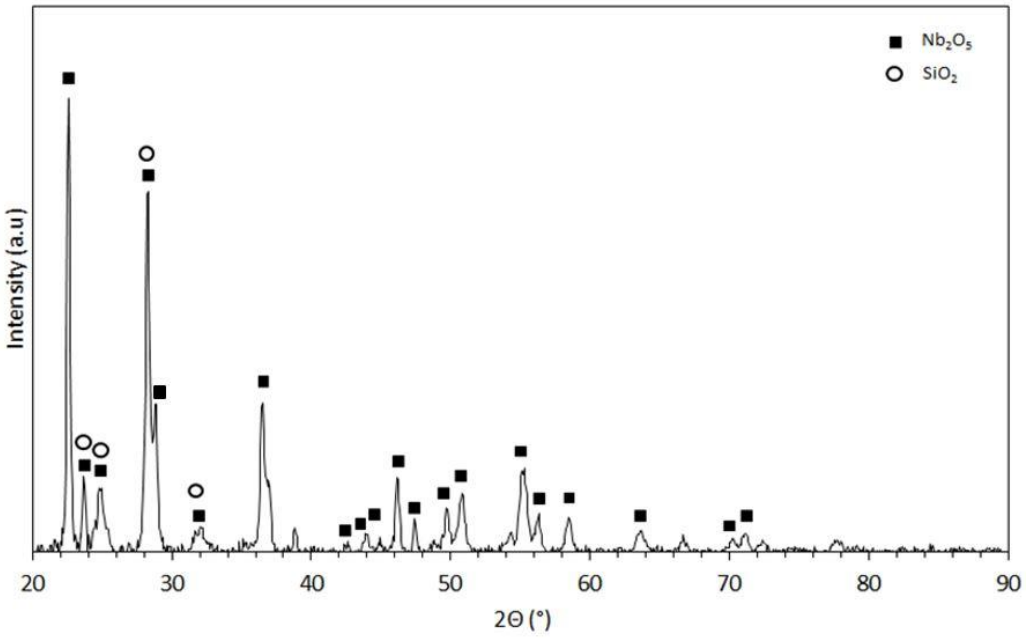

Figure 4.9: XRD pattern of combustion product of the mixture with Nb/Si mole ratio of 3 after oxidation in TGA.

4.2.2 Thermogravimetric Analysis

For comparison, TGA oxidation tests were first conducted with the initial Nb/Si mixtures. Figure 4.10 shows the obtained TG curves at 10°C/min. It is seen that oxidation progressed sharply upon reaching a temperature of about 470 °C.

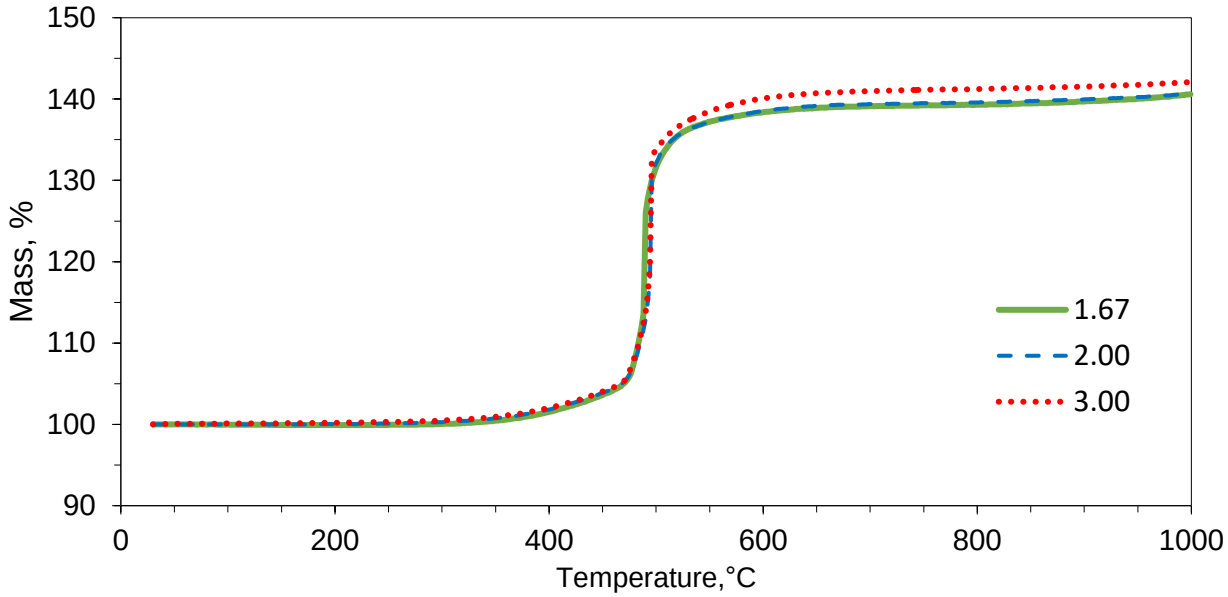

Figure 4.10: TG curves for oxidation of the initial Nb/Si mixtures with Nb/Si mole ratios of 1.67, 2, and 3.

Figures 4.11 − 4.13 show the TG curves for oxidation of the Nb/Nb_5Si_3 products obtained from the mixtures with different Nb/Si mole ratios. For all the samples, oxidation started at about 500 °C. It is seen that at lower heating rates, the oxidation occurs at lower temperatures. The products were fully oxidized at about 750 °C at 1 °C/min and at about 800 °C at 10 °C/min. Testing small pieces of the product pellets with no grinding produced similar results. The products possessing a higher concentration of niobium have demonstrated a slightly lower mass gain during the non-isothermal oxidation.

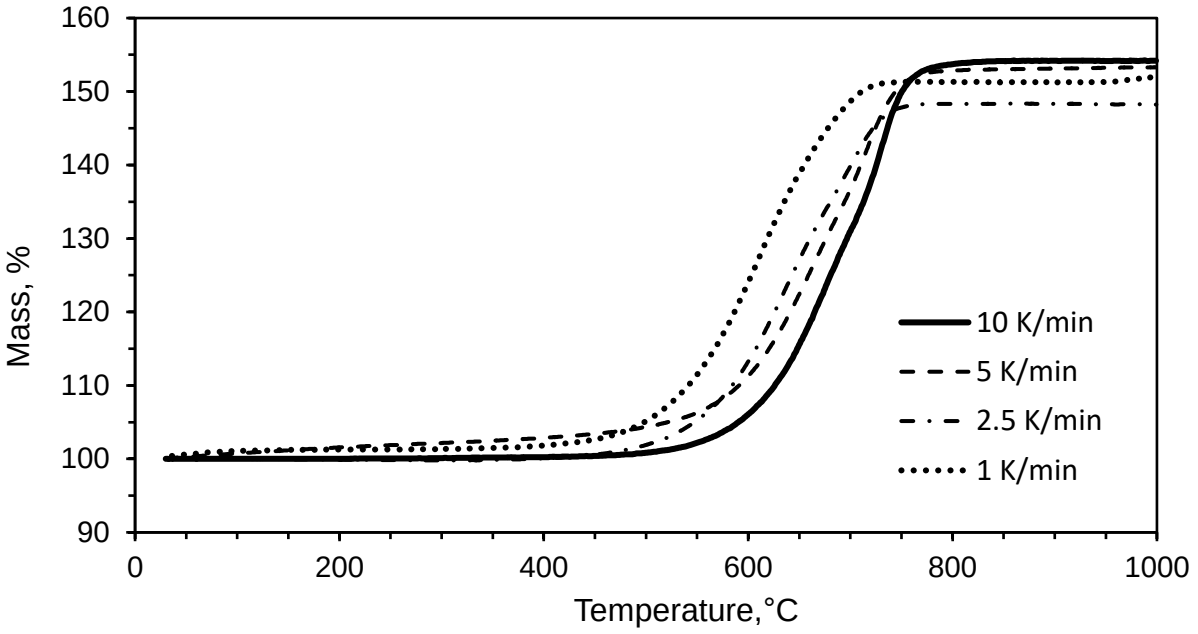

Figure 4.11: TG curves for oxidation of the products obtained from the mixtures with Nb/Si mole ratio of 1.67, at the heating rates of 10, 5, 2.5, and 1 °C/min.

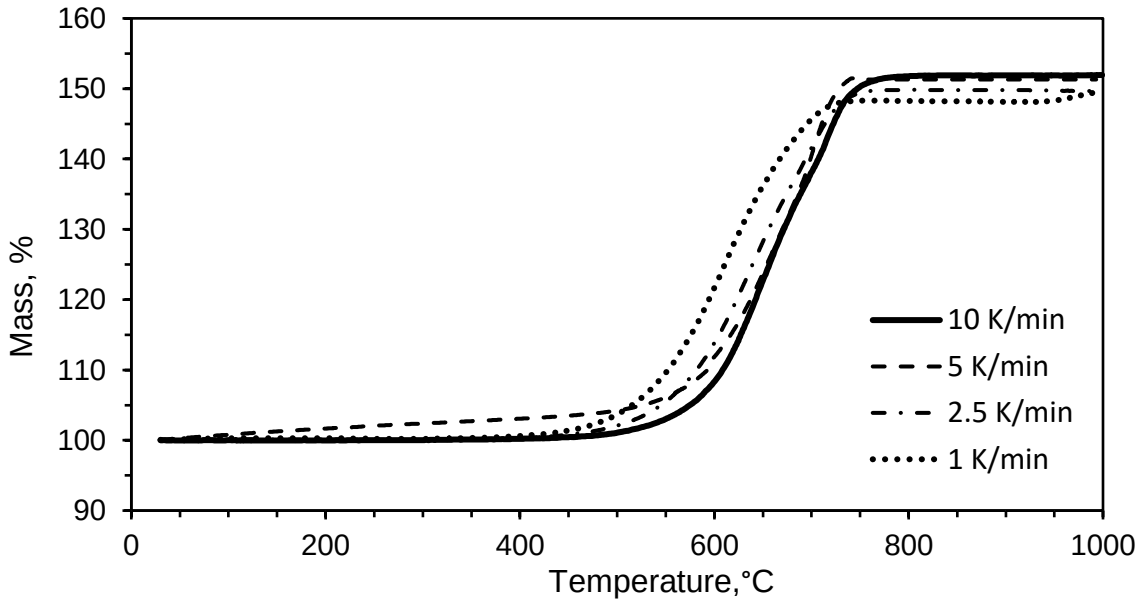

Figure 4.12: TG curves for oxidation of the products obtained from the mixtures with Nb/Si mole ratio of 2 at the heating rates of 10, 5, 2.5, and 1 °C/min.

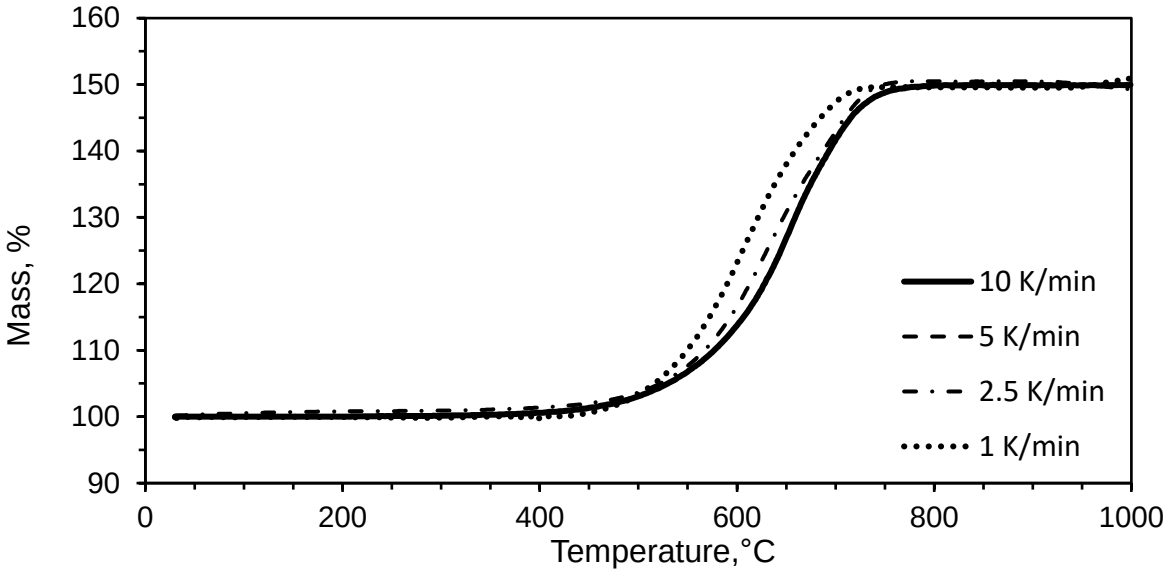

Figure 4.13: TG curves for oxidation of the products obtained from the mixtures with Nb/Si mole ratio of 3 at heating rates of 10, 5, 2.5, and 1 °C/min.

Table 4.1 presents the temperature that corresponds to 50% of the mass change, the measured mass change at heating rates of 10 °C/min and 1 °C/min, and the theoretical mass change calculated for full oxidation. The latter was calculated using Eqs. (4) and (5), i.e. assuming oxidation to Nb_2O_5 and SiO_2. It is seen that temperatures at 50% of the mass change are lower at 1 °C/min (606 °C – 610°C) than at 10 °C /min (645 °C – 688 °C). The difference between the measured and theoretical values of the mass change is within 5%, which indicates that full oxidation took place.

Table 4.1: Thermogravimetric parameters for oxidation of products obtained by combustion of Nb/Si mixtures.

Nb/Si Mole Ratio	Temperature at 50% of the Mass Change		Experimental Mass Change		Theoretical Mass Change
	10 °C/min	1 °C/min	10 °C/min	1 °C/min	
	°C	°C	%	%	%
1.67	688	606	54.2	51.9	53.9
2	660	610	51.9	49.6	52.4
3	645	607	49.9	50.9	49.5

4.2.3 Determination of Kinetic Parameters

The apparent activation energy and pre-exponential factor of the oxidation reaction were extracted from the TGA data for Nb_5Si_3 products (i.e. those obtained from Nb/Si mixtures with Nb:Si mole ratio of 1.67:1), using the Ozawa-Wall-Flynn method and Netzsch Thermokinetics 3.1 software. Figure 4.14 shows the dependencies of the logarithm of the heating rate on the reciprocal of the temperature at different values of the conversion degree. As seen from Eq. (7), the activation energy is proportional to the slope of such a dependence. Using Eqs. (7) and (8), the software calculated the dependencies of the activation energy and pre-exponential factor on the conversion degree, shown in Fig. 4.15. It is seen that the variation of the kinetic parameters is relatively small in the range of conversion degrees 0.2 – 0.7. This is also seen in Table 4.2, which presents their values at different conversion degrees.

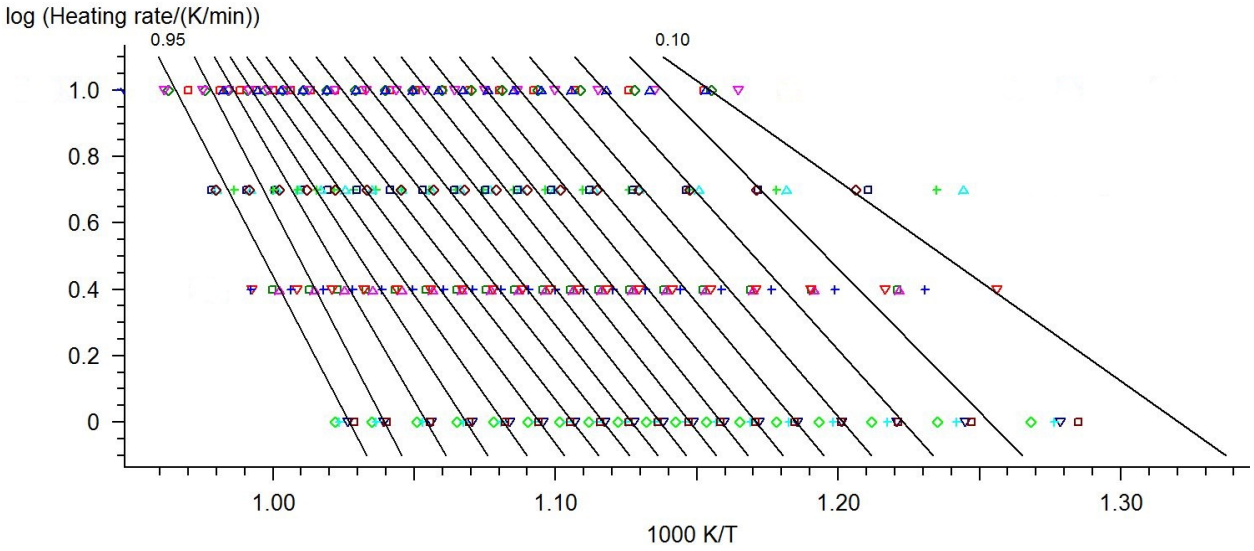

Figure 4.14: The heating rate vs. the reciprocal of the temperature at different conversion degrees 0.05 apart.

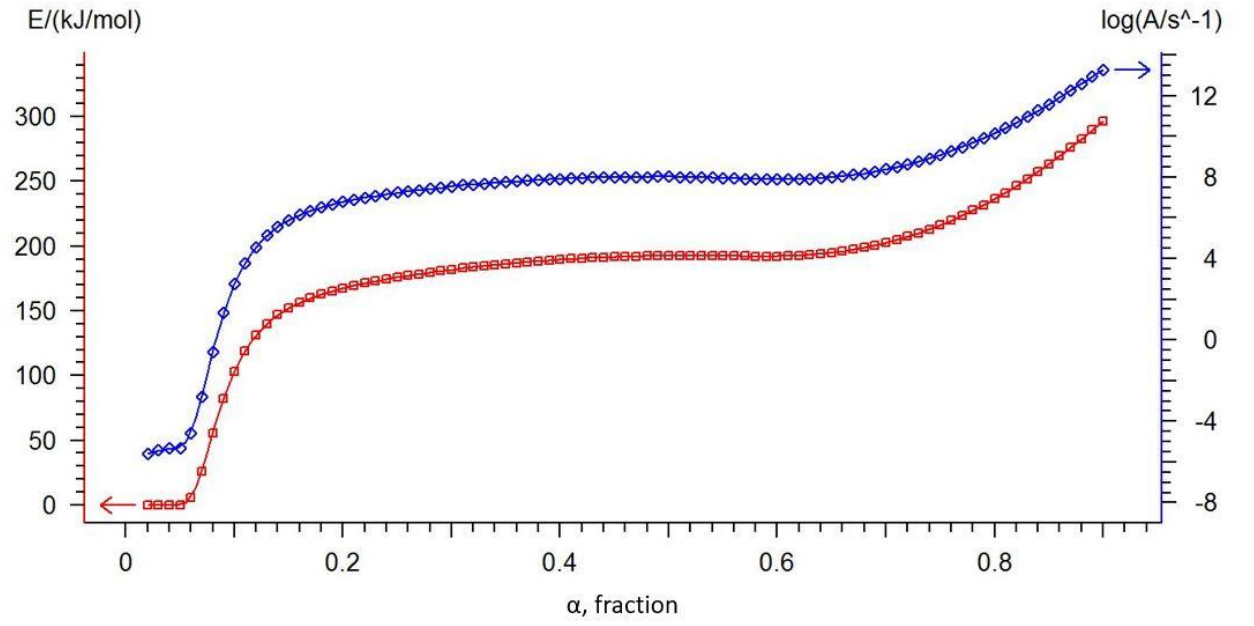

Figure 4.15: The activation energy (red) and the pre-exponential factor (blue) vs. the conversion degree.

Table 4.2: The activation energy and the pre-exponential factor at different conversion degrees.

α	***E*, kJ/mol**	**log (*A*/s^{-1})**	***A*, s^{-1}**
0.05	0.1 ± 1.9	-5.3	$5.01 \cdot 10^{-6}$
0.1	103.3 ± 24.3	2.75	$5.62 \cdot 10^{2}$
0.2	167.5 ± 13.3	6.78	$6.03 \cdot 10^{6}$
0.3	181.9 ± 10.9	7.55	$3.55 \cdot 10^{7}$
0.4	189.6 ± 10.7	7.92	$8.32 \cdot 10^{7}$
0.5	192.9 ± 11.0	8.02	$1.05 \cdot 10^{8}$
0.6	192.2 ± 11.6	7.89	$7.76 \cdot 10^{7}$
0.7	202.7 ± 11.6	8.39	$2.45 \cdot 10^{8}$
0.8	236.4 ± 12.7	10.16	$1.45 \cdot 10^{10}$
0.9	296.5 ± 19.3	13.29	$1.95 \cdot 10^{13}$

Since the Ozawa-Wall-Flynn method requires independency of the kinetic parameters on the conversion degree, an accurate determination of the activation energy and pre-exponential factor based on the obtained data is impossible. However, one can suggest that the apparent activation energy is in the range from 150 to 200 kJ/mol. It should be noted that the Ozawa-Wall-Flynn method assumes the first order of the reaction and does not allow to make any conclusions about the actual reaction mechanism. The dependence of the activation energy on the conversion degree may reflect the complex mechanism of the reaction.

A model-based analysis of the obtained TGA data for oxidation of only the Nb/Si mole ratio of 1.67 was conducted using Thermokinetics 3.1 software. Based on the TGA results, a one-stage model was tested. The determination of the activation energy is an iterative process, and is

advised to perform calculations using all models initially. The software then outputs a graph of measured and calculated curves using the linear regression method. Table 4.3 presents four models that fit the experimental curves with different degrees of accuracy (the best is characterized by F_{exp} = 1) and their kinetic parameters. It is seen that the last two models in the table are characterized by significantly larger values of F_{exp}, which indicates a worse fit. For this reason, these models are excluded from subsequent analysis.

Table 4.3: Kinetic models and their parameters determined in model-based analysis of the TGA data on the oxidation of Nb/Nb_5Si_3 composites.

Model	E_a, **kJ/mol**	A, s^{-1}	n	F_{exp}
An	193	$8.1 \cdot 10^8$	0.55	1.00
D3	212	$9.1 \cdot 10^9$	-	1.03
D4	190	$6.4 \cdot 10^8$	-	1.28
D1	181	$1.9 \cdot 10^8$	-	1.41

According to the F-test, the Avrami-Erofeev nucleation model (An) provides the best fit with the experimental TG data on the oxidation of Nb/Nb_5Si_3 composites. Figure 4.16 shows calculated TG curves for this model in comparison with the experimental dependencies. The oxidation begins with the adsorption of oxygen on the substrate surface, which then diffuses into the substrate as the reaction proceeds. This leads to the formation of an oxide on the surface as a layer or as a separate nucleus [44-46]. Nucleation may occur during the oxidation of both the niobium and niobium silicides, leading to the formation of Nb_2O_5 and SiO_2.

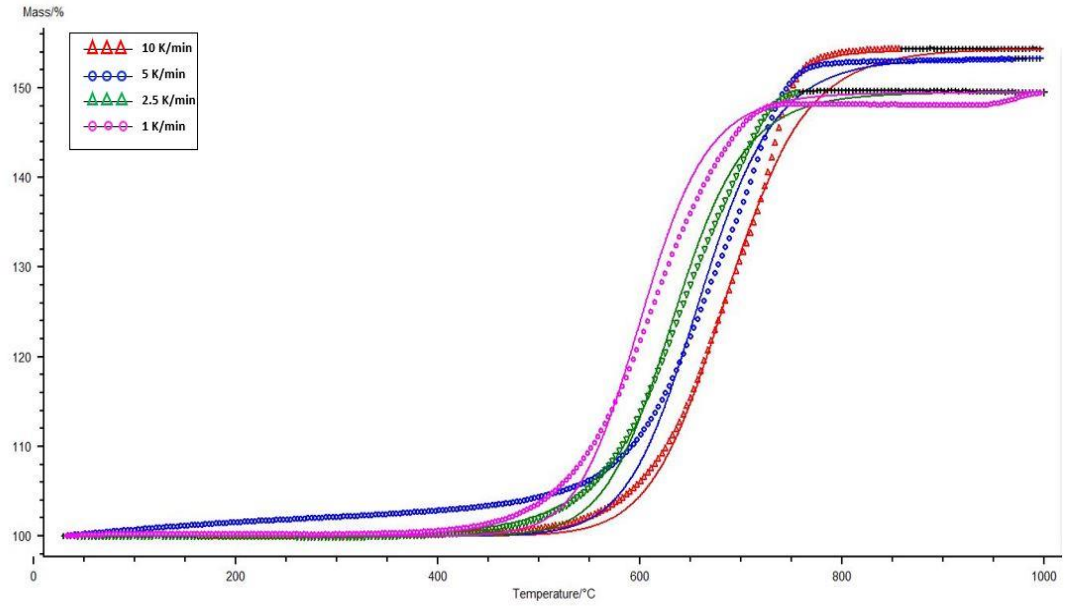

Figure 4.16: Experimental (points) and predicted (lines) TG curves. Kinetic model: An.

The second best (according to the F-test) model that can describe the oxidation process of Nb/Nb_5Si_3 composites is three-dimensional diffusion, described by Jander's equation (D3). Figure 4.17 shows calculated TG curves for this model in comparison with the experimental dependencies. As noted above, the oxidation mechanism of niobium involves the adsorption of dissociated oxygen on the metal surface, followed by diffusion of oxygen through the oxide layer and oxide nucleation. The oxidation process is described by parabolic (at temperatures lower than 500 °C) and linear (at 500 – 800 °C) laws [44,47,48]. The growth of the oxide scale is controlled by diffusion of ions involved in the oxidation process [49].

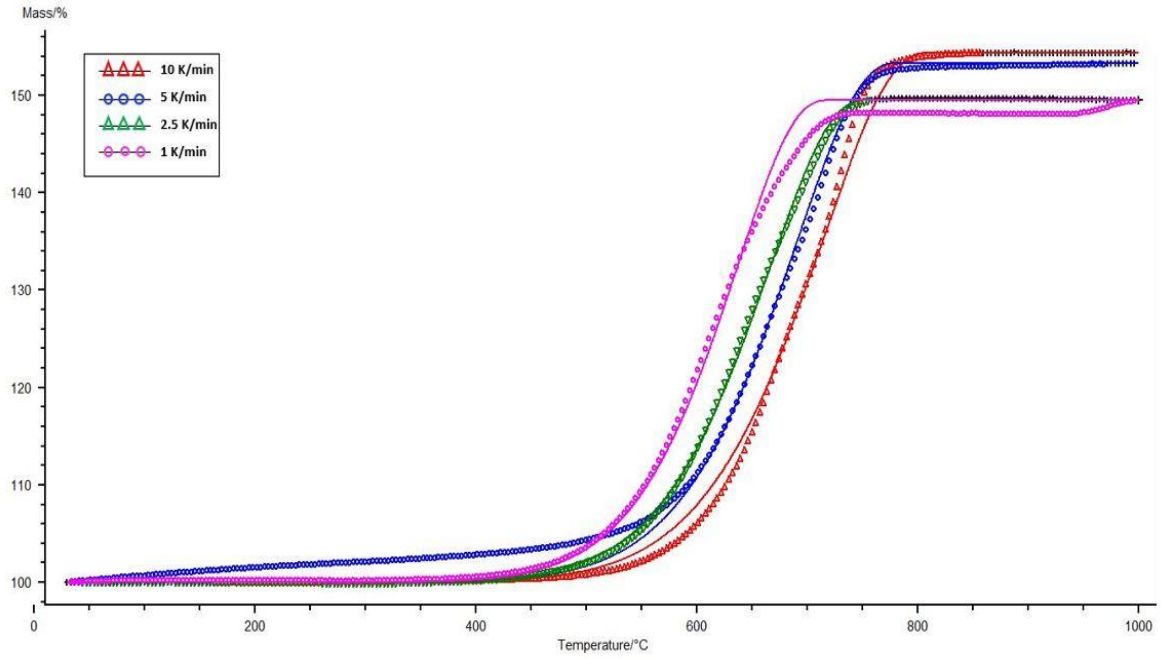

Figure 4.17: Experimental (points) and predicted (lines) TG curves. Kinetic model: D3.

Summarizing, the oxidation kinetics of the obtained Nb/Nb_5Si_3 composites could be described by the Avrami-Erofeev nucleation (An) and the three-dimensional diffusion (D3) models. Each model reflects components of the oxidation mechanism such as nucleation and diffusion. The analysis of the obtained TG does not allow one to make an unambiguous choice. Both models, however, predict similar values of the apparent activation energy, 193 and 212 kJ/mol (see Table 4.3).

4.2.4 Differential Scanning Calorimetry

Figure 4.18 shows the DSC curves for the oxidation of the obtained Nb/Nb_5Si_3 products. The heating rate was 10 °C/min. A prominent exotherm was observed between 600 and 800 °C, which corresponds to the mass increase in the TG curves in Figures 4.11 − 4.13. The temperature rise in this peak is not smooth; it includes two inflection points, which could be considered as an additional peak, especially in the curve for the products obtained from the stoichiometric (5:3)

Nb/Si mixture. This implies that the oxidation is a two-stage process, which may explain the fact that the activation energy depended on the conversion degree in the Ozawa-Wall-Flynn analysis of the TGA data.

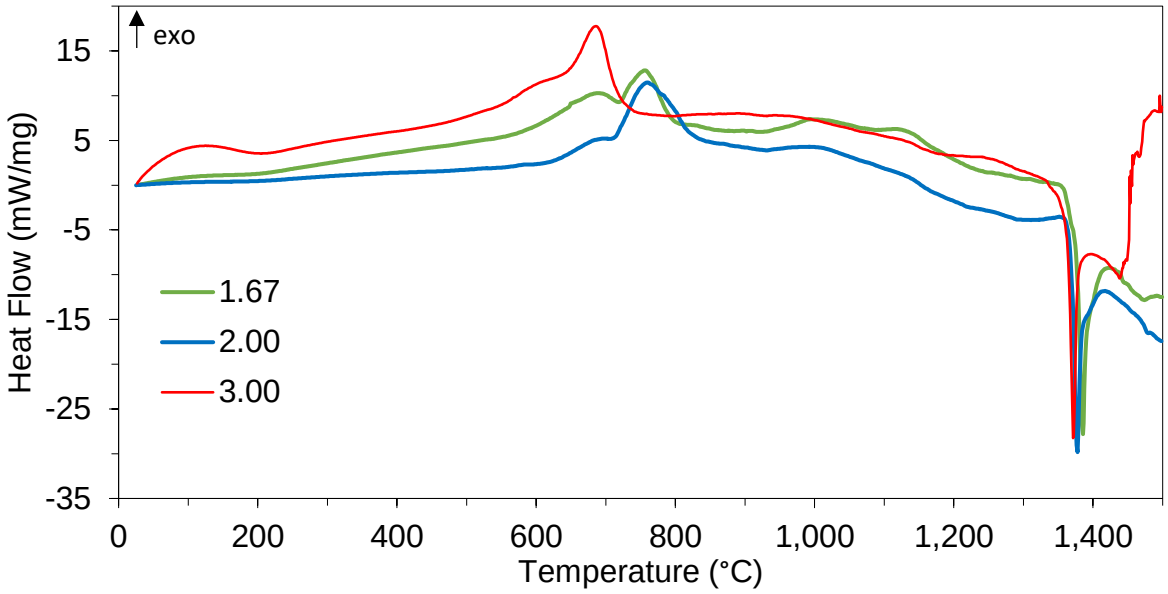

Figure 4.18: DSC curves for oxidation of the products obtained from the mixtures with Nb/Si mole ratios of 1.67, 2, and 3. Heating rate: 10 °C/min.

A strong endothermic peak was observed at 1371 – 1372 °C. This may be explained by the formation and melting of Nb_2O_5 – SiO_2 – Si eutectic composition (the melting points of these materials are 1512 °C, 1710 °C, and 1414 °C, respectively). Unexpectedly, in the product obtained from the mixture with Nb:Si = 3.00, at 1440 °C a high exotherm began. Apparently, this was caused by oxidation of Si that remained unreacted in this particular experiment.

Chapter 5: Conclusions

The products of the stoichiometric (Nb:Si = 5:3 mole ratio) mixture contain α-Nb_5Si_3, γ-Nb_5Si_3, and traces of Nb_3Si. As the concentration of niobium increased, the content of γ phase in the products decreased. The scanning electron microscopy of the products revealed a porous surface of the material, consisting of Nb_{ss} and Nb_5Si_3 phases.

Oxidation of the obtained Nb_5Si_3/Nb composites was studied using non-isothermal TGA and DSC. For all the samples, oxidation started at about 500 °C. The products were fully oxidized at about 750 °C at a heating rate of 1 °C/min and at about 800 °C at 10 °C/min. The Ozawa-Wall-Flynn analysis of the TGA data has shown that the activation energy depends on the conversion degree, which prevented reliable conclusions on the kinetics. In model-based analysis of the TGA data, the Avrami-Erofeev *n*-dimensional nucleation model and three-dimensional diffusion model exhibited the best fit with the TG curves. These models reflect different components of the oxidation mechanism, such as nucleation and diffusion, and predict similar values of the apparent activation energy, 193 and 212 kJ/mol, respectively.

The DSC revealed a prominent exotherm between 600 and 800 °C, which corresponds to the mass increase in the TG curves. The temperature rise in this peak is not smooth; it includes two inflection points, which could be considered as an additional peak. This implies that the oxidation may be a two-stage process, which may explain the fact that the activation energy depended on the conversion degree in the Ozawa-Wall-Flynn analysis of the TGA data.

Summarizing, the results indicate the Nb_5Si_3/Nb composites obtained by MASHS have low resistance to oxidation at temperatures above 500 °C. Additives and protective coatings are necessary for improving the oxidation resistance of these materials.

References

[1] Padture, N. P. (2002). Thermal Barrier Coatings for Gas-Turbine Engine Applications. *Science*, *296*(5566), 280–284. doi: 10.1126/science.1068609

[2] Perepezko, J. H. (2009). The Hotter the Engine, the Better. *Science, 326*(5956), 1068-1069. doi: 10.1126/science.1179327

[3] Bewlay, B. P., Jackson, M. R., Subramanian, P. R., and Zhao, J. -C. (2003). A Review of Very-Tigh-Temperature Nb-Silicide-based Composites. *Metallurgical and Materials Transactions A, 34*(10), 2043-2052. doi: 10.1007/s11661-003-0269-8

[4] Bewlay, B. P., Jackson, M. R., Zhao, J., Subramanian, P. R., Mendiratta, M. G., and Lewandowski, J. J. (2003). Ultrahigh-Temperature Nb-Silicide-Based Composites. *MRS Bulletin, 28*(9), 646-653. doi: 10.1557/mrs2003.192

[5] Bewlay, B. P., Jackson, M. R., and Gigliotti, M. F. (2002). Niobium Silicide High Temperature In Situ Composites. In: *Intermetallic Compounds - Principles and Practice, Volume 3,* Edited by Westbrook J. H., and Fleischer, R.L., New York: Wiley, pp. 541-560. doi: 10.1002/0470845856.ch26

[6] Morsi, K. (2011). The Diversity of Combustion Synthesis Processing: A Review. *Journal of Materials Science, 47*(1), 68-92. doi: 10.1007/s10853-011-5926-5

[7] Shtansky, D. V. (2017). Materials and Coatings for High-Temperature Applications. *Concise Encyclopedia of Self-Propagating High-Temperature Synthesis,* 188-189. doi: 10.1016/b978-0-12-804173-4.00087-9

[8] Sarkisyan, A. R., Dolukhanyan, S. K., and Borovinskaya, I. P. (1978). Self-Propagating

High-Temperature Synthesis of Transition Metal Silicides. *Soviet Powder Metallurgy and Metal Ceramics, 17*(6), 424-427. doi: 10.1007/bf00795793

[9] Sarkisyan, A. R., Dolukhanyan, S. K., and Borovinskaya, I. P. (1979). Investigation of Processes of the Combustion of Hafnium, Niobium, and Tantalum with Silicon. *Combustion, Explosion, and Shock Waves, 15*(1), 95-97. doi: 10.1007/bf00785339

[10] Arkhangel'skii, I. V., Dunaev, A. V., Makarenko, I. V., Tikhonov, N. A., Belyaev, S. S., and Tarasov, A. V. (2013). *Non-Isothermal Kinetic Methods*, Berlin: Edition Open Access, Max Planck Research Library for the History and Development of Knowledge. Retrieved from https://www.mprl-series.mpg.de/textbooks/1/index.html

[11] Schlesinger, M. E., Okamoto, H., Gokhale, A. B., and Abbaschian, R. (1993). The Nb-Si (Niobium-Silicon) System. *Journal of Phase Equilibria, 14*(4), 502-509. doi: 10.1007/BF02671971

[12] Bewlay, B. P., Whiting, P. W., Davis, A. W., and Briant, C. L. (1998). Creep Mechanisms in Niobium-Silicide Based In-Situ Composites. *MRS Proceedings, 552*. doi: 10.1557/proc-552-kk6.11.1

[13] Bewlay, B. P., Jackson, M. R., and Lipsitt, H. A. (1996). The Balance of Mechanical and Environmental Properties of a Multielement Niobium-Niobium Silicide-BasedIn Situ Composite. *Metallurgical and Materials Transactions A, 27*(12), 3801-3808. doi: 10.1007/bf02595629

[14] Bewlay, B., Lipsitt, H., Jackson, M., Reeder, W., and Sutliff, J. (1995). Solidification Processing of High Temperature Intermetallic Eutectic-Based Alloys. *Materials Science and Engineering A, 192-193*, 534-543. doi: 10.1016/0921-5093(95)03299-1

[15] Cockeram, B., Srinivasan, R., and Weiss, I. (1992). The Effect of Nb_3Si Precipitates on the Deformation of the Primary Nb Phase in Nb-10 a/o Si In-Situ Composite. *Scripta Metallurgica et Materialia, 26*(5), 755-760. doi: 10.1016/0956-716x(92)90433-f

[16] Cockeram B., Saqib M., Omlor R., Srinivasan R., Watson L.E., and Weiss I. (1991), Characterization of Silicide Precipitates in Primary Nb Phase in Nb-10%Si In-Situ Composites, *Scripta Metallurgica et Materialia*, *25*, 393-398

[17] Yonghua, D. (2015). Stability, Elastic Constants and Thermodynamic Properties of (α, β, γ)-Nb5Si3 Phases. *Rare Metal Materials and Engineering, 44*(1), 18-23. doi: 10.1016/s1875-5372(15)30004-7

[18] Bewlay B. P. and Jackson M. R. (1997), The Nb-Ti-Si Ternary Phase Diagram: Determination of Solid-State Phase Equilibria in Nb-and Ti-Rich Alloys, *Journal of Phase Equalibria*, *18*(3), 264-278.

[19] Bewlay B. P. and Jackson M. R. (1998), The Nb-Ti-Si Ternary Phase Diagram: Determination of Solid-State Phase Equilibria in Nb-and Ti-Rich Alloys, *Journal of Phase Equilibria*, *19*(6) 577-586.

[20] Bewlay B. P., Jackson M. R., Reeder W. J., and Lipsitt H. A. (1995), Microstructures and Properties of DS In-Situ Composites of Nb-Ti-Si Alloys, *MRS Symposium Proceedings*, *364*, 943-948.

[21] Zhao J. C., Bewlay B. P., and Jackson M. R. (2001), Determination of Nb-Hf-Si Phase Equilibria, in: *Structural Intermetallics*, Edited by Hemker K. J., Dimiduk D. M., Clemens H., Darolia R., Inui H., Larsen J. M., Sikka V. K., Thomas M. and Whittenberger J. D., The Minerals, Metals & Materials Society, pp. 681-689.

[22] Zhao J.C., Bewlay B. P., Jackson M. R., and Peluso L. A. (2001), Alloying and Phase Stability in Niobium Silicide In-Situ Composites, in: *Structural Intermetallics*, Edited by Hemker K. J., Dimiduk D. M., Clemens H., Darolia R., Inui H., Larsen J. M., Sikka V. K., Thomas M. and Whittenberger J. D., The Minerals, Metals & Materials Society, pp. 483-491.

[23] Kang, Y., Qu, S., Song, J., Huang, Q., and Han, Y. (2012). Microstructure and Mechanical Properties of Nb–Ti–Si–Al–Hf–xCr–yV Multi-Element In-Situ Composite. *Materials Science and Engineering A, 534*, 323-328. doi: 10.1016/j.msea.2011.11.076

[24] Guo, Y., Jia, L., Sun, S., Kong, B., Liu, J., and Zhang, H. (2016). Rapid fabrication of Nb-Si Based Alloy by Selective Laser Melting: Microstructure, Hardness and Initial Oxidation Behavior. *Materials & Design*, *109*, 37–46. doi: 10.1016/j.matdes.2016.07.048

[25] Mendiratta, M. G., Lewandowski, J. J., and Dimiduk, D. M. (1991). Strength and Ductile-Phase Toughening in the Two-Phase Nb/Nb_5Si_3 alloys. *Metallurgical Transactions A*, *22*(7), 1573–1583. doi: 10.1007/bf02667370

[26] Fu, Y., Liu, W., Zong, W., and Sha, J. (2012). Microstructure and Room-Temperature Mechanical Properties of Nb/Nb_5Si_3 Alloys Fabricated by Spark Plasma Sintering. *Procedia Engineering*, *27*, 1156–1161. doi: 10.1016/j.proeng.2011.12.566

[27] Kofstad, P. (1988). *High Temperature Corrosion*. London/New York: Elsevier Applied Science.

[28] Semmel, J. W. (1961). *Refractory Metals and Alloys: Proceedings of a Technical Conference Sponsored by the Refractory Metals Committee of the Institute of Metals Division, the Metallurgical Society, and Detroit Section, American Institute of Mining, Metallurgical and*

Pteroleum Engineers, Detroit, Michigan, May 25-26, 1960. New York: Interscience.

[29] Birks, N., Meier, G. H., and Pettit, F. S. (2009). *Introduction to the High-Temperature Oxidation of Metals*. Cambridge: Cambridge University Press.

[30] Kofstad, P., and Steidel, C. A. (1967). High Temperature Oxidation of Metals. *Journal of The Electrochemical Society*, *114*(7). doi: 10.1149/1.2426698

[31] Arbuzov, M. P., and Chuprina, V. G. (1966). The Oxidation of Niobium and the Structure of Niobium Oxides. *Soviet Physics Journal*, *8*(2), 87–89. doi: 10.1007/bf00838593

[32] Sheasby, J. S., and Smeltzer, W. W. (1981). Oxygen Tracer Studies of the Oxidation of Niobium. *Oxidation of Metals*, *15*(3-4), 215–229. doi: 10.1007/bf01058826

[33] Song, B., Feng, P., Wang, J., Ge, Y., Wu, G., Wang, X., and Akhtar, F. (2014). Oxidation Properties of Self-Propagating High Temperature Synthesized Niobium Disilicide. *Corrosion Science*, *85*, 311–317. doi: 10.1016/j.corsci.2014.04.029

[34] Guo, Y., Jia, L., Kong, B., Zhang, F., Liu, J., and Zhang, H. (2017). Improvement in the Oxidation Resistance of Nb-Si Based Alloy by Selective Laser Melting. *Corrosion Science*, *127*, 260–269. doi: 10.1016/j.corsci.2017.08.022

[35] Chattopadhyay, K., Mitra, R., and Ray, K. (2008). Nonisothermal and Isothermal Oxidation Behavior of Nb-Si-Mo Alloys. *Metallurgical and Materials Transactions A*, *39*(3), 577–592. doi: 10.1007/s11661-007-9398-9

[36] Young, D. J. (2016). *High Temperature Oxidation and Corrosion of Metals*. Oxford: Elsevier.

[37] Duval, C. (1963). *Inorganic Thermogravimetric Analysis*. London: Elsevier.

[38] Geng, J., Tsakiropoulos, P., and Shao, G. (2007). A Thermo-Gravimetric and Microstructural Study of the Oxidation of Nbss/Nb_5Si_3-Based In-Situ Composites with Sn Addition. *Intermetallics*, *15*(3), 270–281. doi: 10.1016/j.intermet.2006.06.003

[39] Haines, P. J. (1995). *Thermal Methods of Analysis: Principles, Applications and Problems*. London: Blackie Academic.

[40] Shamim, M., Mukhopadhyay, T. K., and Dana, K. (2015). Kinetic Pathway for Thermal Exfoliation of Pyrophyllite. *Applied Clay Science, 114*, 40-47. doi: 10.1016/j.clay.2015.05.006

[41] Ozawa, T. (1965). A New Method of Analyzing Thermogravimetric Data. *Bulletin of the Chemical Society of Japan*, *38*(11), 1881–1886. doi: 10.1246/bcsj.38.1881

[42] Blaine, R. L., and Kissinger, H. E. (2012). Homer Kissinger and the Kissinger Equation. *Thermochimica Acta*, *540*, 1–6. doi: 10.1016/j.tca.2012.04.008

[43] *E1641-18 Standard Test Method for Decomposition Kinetics by Thermogravimetry Using the Ozawa/Flynn/Wall Method*. (2018). West Conshohocken, PA: ASTM International. doi: 10.1520/E1641-18

[44] Mansurova, A. N., Gulyaeva, R. I., and Chumarev, V. M. (2017). Kinetic Analysis of the Oxidation of Nb–Si Eutectic Alloy Doped with Boron. *Inorganic Materials: Applied Research*, *8*(2), 318–326. doi: 10.1134/s2075113317020150

[45] Zhou, G. (2009). Nucleation Thermodynamics of Oxide During Metal Oxidation. *Applied Physics Letters*, *94*(20), 201905. doi: 10.1063/1.3141511

[46] George, R., and Sugunan, S. (2014). Kinetics of Adsorption of Lipase onto Different

Mesoporous Materials: Evaluation of Avrami Model and Leaching Studies. *Journal of Molecular Catalysis B: Enzymatic*, *105*, 26–32. doi: 10.1016/j.molcatb.2014.03.008

[47] Xu, J., Zhao, X., and Gong, S. (2007). The Influence of Nb Diffusion on the Oxidation Behavior of TiNiAlNb Alloys with Different Ti/Ni Ratio. *Materials Science and Engineering: A*, *458*(1-2), 381–384. doi: 10.1016/j.msea.2006.12.085

[48] Perkins, R. A., and Meier, G. H. (1990). The Oxidation Behavior and Protection of Niobium. *JOM, 42*(8), 17-21. doi: 10.1007/bf03221046

[49] Mitra, R. (2019). Oxidation Behavior of Silicides. *Diffusion Foundations, 21*, 127-156. doi: 10.4028/www.scientific.net/df.21.127

Vita

Frank A. Perez was born in El Paso, Texas. He received his Bachelor of Science in Mechanical Engineering from the University of Texas at El Paso (UTEP) in December 2018. At the end of his senior year, he worked as an undergraduate research assistant of Dr. Luis Echegoyen under the NSF Partnership for Research and Education in Materials Research (NSF-PREM) program. In January 2019, Mr. Perez began his graduate studies at UTEP toward his master's degree in Mechanical Engineering under the supervision of Dr. Evgeny Shafirovich. His master's studies focused on oxidation of niobium silicides fabricated by self-propagating high-temperature synthesis. Over the past three years, Mr. Perez has co-authored 4 journal publications.

E-mail: faperez2@miners.utep.edu